

# Generalization of Anisotropic Damage Mechanics Modeling in the Material Point Method

John A. Nairn\*

*Wood Science and Engineering, Oregon State University, Corvallis, OR 97330, USA*

## SUMMARY

Anisotropic damage mechanics is derived by redefining its fourth-ranked damage tensor,  $\mathbf{D}$ , not by its effect on stiffness reduction, but as a tensor that partitions total strain into bulk material strain and an cracking strain associated with crack-opening displacement. This re-characterization of  $\mathbf{D}$  is irrelevant for 1D modeling, but significantly clarifies 3D algorithms. The new 3D derivation starts with three damage parameters associated with three independent strength models for three components of crack traction. By postulating a traction failure surface dependent on current damage state and requiring that all traction components simultaneously decay to zero at failure, the three damage parameters naturally couple to a single parameter. Many prior methods assume evolving strength depends only on damage. In real materials, strength often depends on other variables such as temperature, pressure, strain rate, and so forth. This paper proposes a new general theory that extends prior methods to properly account for such external variables. The general damage mechanics methods must account for extra variables during damage initiation, damage evolution, and elastic loading and unloading. Several examples focus on the new concepts for coupling damage parameters and for using general methods to model materials with pressure-dependent strength properties. Copyright © 2022 John Wiley & Sons, Ltd.

First published: 09 May 2022

KEY WORDS: Damage Mechanics; Fracture; Particle methods

## 1. INTRODUCTION

Damage mechanics has a long history of modeling failure by introducing damage parameters characterizing the damage [1]. In one general form, damage mechanics relates stress ( $\boldsymbol{\sigma}$ ) to strain ( $\boldsymbol{\varepsilon}$ ) using

$$\boldsymbol{\sigma} = (\mathbf{I} - \mathbf{D}^T) \mathbf{C} (\boldsymbol{\varepsilon}_{total} - \boldsymbol{\varepsilon}_{res}) = (\mathbf{I} - \mathbf{D}^T) \mathbf{C} \boldsymbol{\varepsilon} \quad (1)$$

where  $\mathbf{C}$  is the undamaged material's fourth-rank stiffness tensor,  $\mathbf{D}$  is a fourth-rank damage tensor [2, 3] (the reason for transpose is explained below),  $\boldsymbol{\varepsilon}_{total}$  is total strain, and  $\boldsymbol{\varepsilon}_{res}$  is residual strain caused by changes in temperature, solvent content, or other similar effects. The final form fully accounts for residual strain effects by using a *net* strain  $\boldsymbol{\varepsilon} = \boldsymbol{\varepsilon}_{total} - \boldsymbol{\varepsilon}_{res}$ .

Equation (1) defines an effective stiffness  $\mathbf{C}_{eff} = (\mathbf{I} - \mathbf{D}^T) \mathbf{C}$ , which implies  $\mathbf{D}$  models stiffness reductions (or softening) caused by damage. In general,  $\mathbf{C}_{eff}$  will soften differently in different directions (depending on the form of  $\mathbf{D}$ ). This style of damage mechanics is therefore referred to as “anisotropic damage mechanics” (ADaM) where anisotropy refers to the changes in stiffness and not the underlying undamaged material, which may be either isotropic or anisotropic [2, 3].

Damage mechanics analysis can also be viewed as partitioning total strain,  $\boldsymbol{\varepsilon}$ , into a sum of elastic strain on the material,  $\boldsymbol{\varepsilon}_e$ , and damage strain,  $\boldsymbol{\varepsilon}_d$ . The elastic strain leads to material

---

\*Correspondence to: Wood Science and Engineering, Oregon State University, Corvallis, OR 97330, USA. Email: John.Nairn@oregonstate.edu

stress while the damage strain characterizes extra strain caused by the damage. When damage mechanics is modeling a crack, the only source of damage strain is crack-opening displacement — to emphasize modeling of cracks,  $\boldsymbol{\varepsilon}_d$  will be referred to here as the cracking strain,  $\boldsymbol{\varepsilon}_c$ . Because effective stiffness must be symmetric, or  $(\mathbf{I} - \mathbf{D}^T)\mathbf{C} = \mathbf{C}(\mathbf{I} - \mathbf{D})$ , the stress derived from elastic strain can be related total strain using

$$\boldsymbol{\sigma} = \mathbf{C}(\mathbf{I} - \mathbf{D})\boldsymbol{\varepsilon} = \mathbf{C}\boldsymbol{\varepsilon}_e = \mathbf{C}(\boldsymbol{\varepsilon} - \boldsymbol{\varepsilon}_c) \quad (2)$$

In other words, the cracking strain is related to total strain by  $\boldsymbol{\varepsilon}_c = \mathbf{D}\boldsymbol{\varepsilon}$ . This form suggests a re-interpretation of  $\mathbf{D}$  as a strain-partitioning tensor that defines the ratio of cracking to total strain. This reinterpretation greatly clarifies development of 3D damage mechanics. Note that Eq. (2) is identical to Eq. (1), but moves damage tensor to opposite side of  $\mathbf{C}$ . As a consequence,  $\mathbf{D}$  defined here is a transpose of  $\mathbf{D}$  in prior ADaM papers [2, 3, 4, 5].

When implementing a numerical (or discrete) model of the above continuum damage mechanics, the body is divided into sufficiently small volume elements. When an element initiates damage, it can be viewed as transversed by a crack with a normal vector,  $\hat{\mathbf{n}}$ , whose orientation is determined by the stress state causing the crack formation. The implementation approach used here is to treat that crack as smeared over the entire element such that cracking strain is determined from crack opening displacement,  $\mathbf{u}^{(cod)}$ , by

$$\boldsymbol{\varepsilon}_c = \frac{1}{2h} \left( (\hat{\mathbf{n}} \otimes \mathbf{u}^{(cod)}) + (\hat{\mathbf{n}} \otimes \mathbf{u}^{(cod)})^T \right) \quad (3)$$

where  $h$  is characteristic dimension of the element [6]. Initial implementation of ADaM in finite elements (FEM) when cracks were fixed at their initial orientation was prone to spurious stresses caused by shear locking [6, 7, 8]. This locking is likely exacerbated by use of constant strain triangles. A FEM-specific mesh correction can improve the modeling [6, 8]. Other FEM approaches have been to revert to isotropic damage mechanics or to base damage evolution on principal stresses rather than crack-plane traction [7, 9]. While such approaches can avoid shear locking caused by FEM meshes, in my opinion they diminish realism of the failure modeling. Isotropic damage mechanics fails to describe material anisotropy caused by cracks. Principal stresses may rotate away from the crack plane and therefore cannot be used to model differences between tensile and shear stresses along the crack plane (*i.e.*, mode I and mode II fracture).

An alternate approach is to switch to a method that does not use FEM. The anisotropic damage mechanics in this paper switches to the material point method (MPM) where the small volume elements are cubical particles (or material points). MPM is a hybrid Eulerian-Lagrangian method that appears to avoid shear locking effects. When a particle initiates damage, it develops a crack, a normal vector to the crack is calculated, the crack is assumed to span the entire cross section that single particle, and the crack opening displacements are smeared over the particle's volume using Eq. (3). The subsequent damage evolution is based on crack-surface normal and current crack-surface traction (rather than principal stress schemes). Dividing crack traction into tensile and shear stresses allows the modeling to treat mode I and mode II failure properties as independent material properties. Most prior damage mechanics consider only total fracture energy. The normal component of crack traction is used to allow damage evolution only when in tension and to model crack contact with frictional sliding when in compression. Prior work on ADaM in MPM has been encouraging [10, 11, 12]; this paper elaborates on and generalizes those approaches.

Section 2 derives ADaM from 1D to 3D based on re-interpretation of  $\mathbf{D}$  as strain-partitioning tensor. This reinterpretation must hold under all stress states including during elastic loading or unloading, damage evolution, or post-failure deformation (including crack contact). These derivations start with a “special theory of damage mechanics” that assumes material failure properties depend *only* on the current damage state. Section 2.1 presents a 1D analysis that is similar to many prior 1D damage mechanics models [13, 14], but a new derivation based on strain-partitioning provides insights that clarify extension to 3D. 3D analysis in section 2.2 starts with three damage parameters that are related to damage states normal and tangential to the

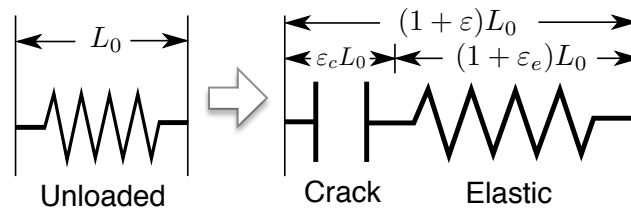


Figure 1. The “unloaded” state is a 1D elastic element with initial length  $L_0$ . After damage initiation, the 1D model has a “crack” element with strain  $\varepsilon_c$ , an “elastic” element with strain  $\varepsilon_e$ , and total strain  $\varepsilon = \varepsilon_c + \varepsilon_e$ .

crack plane. These parameters couple to a single parameter by requiring all traction components to simultaneously decay to zero at failure. The key results are new equations to update damage parameters whenever stress exceeds current strength and partitioning of dissipated energy into tensile and shear failure energy.

Prior damage mechanics models are mostly “special theories,” but that approach has a limitation — it does not account for materials whose failure properties depend on external variables (*e.g.*, temperature, pressure, strain rate, *etc.*). Some prior work has accounted for such effects by changing initiation conditions, but that approach is insufficient. Section 3 derives a new “general theory of damage mechanics,” that extends special theories to allow external variables. The new results show how a general ADaM implementation must account for effects of external variables on initiation, on damage evolution, and on elastic loading and unloading.

Finally, section 4 provides details on MPM implementation of these new methods in custom software [15]. Several examples explore new damage mechanics concepts for coupling damage parameters, compare results to isotropic damage mechanics, and demonstrate general methods to model materials with pressure-dependent failure properties. This section ends with comments about implications of interpreting  $\mathbf{D}$  as a strain-partitioning tensor.

## 2. SPECIAL THEORY OF DAMAGE MECHANICS

### 2.1. One Dimensional Damage Mechanics

This section derives 1D damage mechanics [13, 14] using the strain-partitioning interpretation of  $\mathbf{D}$ . A 1D damage model with an elastic spring element and a strong discontinuity as a crack element is shown in Fig. 1. Stress is found from the spring element while the cracking strain is determined by a scalar damage state parameter,  $D$ , using  $\varepsilon_c = D\varepsilon$ . The 1D constitutive law is  $\sigma = E\varepsilon_e = E(1 - D)\varepsilon$  where  $E$  is the undamaged material’s modulus.

Damage modeling requires a method to evolve  $D$ . One physical approach is to model the crack element in Fig. 1 using a *strength model*,  $F(\delta)$ , for the material’s strength as a function of a second damage variable,  $\delta$ , defined in 1D as the *cracking strain* for which stress equals  $F(\delta)$ .  $\delta$  can be related to  $D$  by solving for strain,  $\varepsilon_i$ , such that 1D stress equals the current strength, and then expressing  $D$  using  $D = \delta/\varepsilon_i$ :

$$\sigma = E(\varepsilon_i - \delta) = F(\delta) \implies \varepsilon_i = \delta + \frac{F(\delta)}{E} \implies D = \frac{\delta}{\varepsilon_i} = \frac{\delta}{\delta + \frac{F(\delta)}{E}} \quad (4)$$

By this equation, damage can be tracked using either  $D$  or  $\delta$ .  $D$  evolves from 0 to 1 and is related to energy dissipation. In contrast,  $\delta$  is related to *maximum* crack opening displacement,  $u_{max}^{(COD)} = \delta L_0$ , and it evolves from zero to  $\delta^{(c)} = u^{(c)}/L_0$  where  $u^{(c)}$  is the material’s critical crack-opening displacement.

Numerical implementation of 1D damage mechanics can proceed by tracking maximum strain defined as  $\varepsilon_{max} = \max(\varepsilon_0, \varepsilon)$  where  $\varepsilon_0$  is strain to initiate damage. Whenever  $\varepsilon_{max}$  increases,  $D$  is updated based on a  $D(\varepsilon_{max})$  damage evolution law and  $\delta = D\varepsilon_{max}$  [13]. While simple in 1D,

this approach does not extend well to 3D. An alternate, but equivalent, implementation is to define a traction failure surface by:

$$\Phi(\sigma, \delta) = \sigma - F(\delta) = E(1 - D)\epsilon - F(\delta)$$

Analogous to yield surfaces in plasticity theory [16],  $\Phi(\sigma, \delta) < 0$  for elastic loading or unloading,  $\Phi(\sigma, \delta) = 0$  during damage evolution, and  $\Phi(\sigma, \delta) > 0$  is not allowed. Given current stress,  $\sigma$ , and an increment in total strain,  $d\epsilon$  (in displacement-driven numerical modeling), if  $\Phi(\sigma^{(trial)}, D) \leq 0$  where  $\sigma^{(trial)} = \sigma + E(1 - D)d\epsilon$ , the increment is elastic. The trial stress is accepted, no changes are made to  $D$  or  $\delta$ , but current cracking strain changes by  $d\epsilon_c = Dd\epsilon$ .

But, if  $\Phi(\sigma^{(trial)}, D) > 0$ , damage evolves. The damage evolution can be determined from a consistency condition:

$$\nabla\Phi(\sigma, \delta) \cdot (d\epsilon, d\delta) = 0 \implies d\delta = \frac{E(1 - D)d\epsilon}{E\epsilon\mathbb{R}(\delta) + F'(\delta)} \tag{5}$$

where  $\mathbb{R}(\delta)$  is ratio of  $D$  evolution to  $\delta$  evolution; it is found from Eq. (4):

$$\mathbb{R}(\delta) = \frac{dD}{d\delta} = \frac{\varphi(\delta)}{E\left(\delta + \frac{F(\delta)}{E}\right)^2} \quad \text{where} \quad \varphi(\delta) = F(\delta) - \delta F'(\delta)$$

Other useful  $\mathbb{R}(\delta)$  forms derived from Eq. (4) are:

$$\mathbb{R}(\delta) = \frac{E(1 - D)^2\varphi(\delta)}{F(\delta)^2} = \frac{(1 - D)D\varphi(\delta)}{\delta F(\delta)} = \frac{D^2\varphi(\delta)}{E\delta^2} = \frac{\sigma D\varphi(\delta)}{\epsilon E\delta F(\delta)} \tag{6}$$

Substituting the second form of  $\mathbb{R}(\delta)$  into Eq. (5) leads to damage increment of

$$d\delta = \frac{d\epsilon}{1 + \frac{F'(\delta)}{E}} \quad \text{and} \quad dD = \mathbb{R}(\delta)d\delta \tag{7}$$

Because cracking strain is equal to  $\delta$  during damage evolution, the increment in 1D cracking strain during damage evolution is trivially  $d\epsilon_c = d\delta$ . As a result,  $\delta$  corresponds to *maximum cracking strain* reached during deformation (but this relation does not extend to 3D). Equation (7) is identical to Ref. [10], but this derivation was simpler and it defines the useful  $\mathbb{R}(\delta)$  function. Finally, Eq. (5) implicitly assumes  $F(\delta)$  is only a function of  $\delta$ . This assumption is what characterizes all special theories of damage mechanics; a general theory needs to remove this assumption.

The tensor  $\mathbf{D}$  is a state parameter describing damage. Whenever  $\mathbf{D}$  is constant, the damaged material's elastic strain energy is

$$U = \frac{1}{2}\boldsymbol{\sigma} \cdot \boldsymbol{\epsilon} = \frac{1}{2}\mathbf{C}(\mathbf{I} - \mathbf{D})\boldsymbol{\epsilon} \cdot \boldsymbol{\epsilon}$$

Whenever  $\mathbf{D}$  changes, energy dissipation,  $d\Omega$ , is caused by a decrease in elastic potential energy,  $\Pi = U - W$ , where  $W$  is external work:

$$d\Omega = -d\Pi = d(W - U) = \boldsymbol{\sigma} d\boldsymbol{\epsilon} - dU = \frac{1}{2}\mathbf{C}d\mathbf{D}\boldsymbol{\epsilon} \cdot \boldsymbol{\epsilon} \tag{8}$$

This energy increment must be zero during elastic deformation and non-negative during damage evolution. In 1D modeling, Eq. (8) gives energy dissipation per unit volume as:

$$d\Omega = \frac{1}{2}E\epsilon^2 dD = \frac{1}{2}E\epsilon^2\mathbb{R}(\delta)d\delta = \frac{1}{2}\varphi(\delta)d\delta \tag{9}$$

The last step used the last form of  $\mathbb{R}(\delta)$  in Eq. (6) and recognized that  $D = \delta/\varepsilon$  and  $\sigma = F(\delta)$  during 1D damage evolution. Energy dissipation up to current  $\delta$  is [10]

$$\bar{G} = \frac{1}{2} \int_0^\delta \varphi(\delta) d\delta = \int_0^\delta F(\delta) d\delta - \frac{\delta F(\delta)}{2}$$

Failure in 1D damage mechanics is characterized by  $D$  reaching 1,  $\delta$  reaching  $\delta^{(c)}$ , or  $\bar{G}$  reaching a material toughness, which all happen simultaneously. At failure,  $F(\delta^{(c)}) = 0$  leading to:

$$\bar{G}_c = \int_0^{\delta^{(c)}} F(\delta) d\delta = \frac{1}{L_0} \int_0^{u^{(c)}} F\left(\frac{u^{(COD)}}{L_0}\right) du^{(COD)} = \frac{G_c}{L_0}$$

where  $G_c$  is the material's fracture mechanics toughness. In other words, area under  $F(\delta)$  is toughness per unit volume while area using crack opening displacement is  $G_c$ . In 3D modeling,  $L_0$  is replaced by  $V/A_c$  where  $V$  is a modeled volume element (e.g., one material point) and  $A_c$  is crack area within that volume element leading to  $\bar{G}_c = G_c A_c / V$  [10].

The strength model  $F(\delta)$  has been left arbitrary. Although many implementations treat  $F(\delta)$  as a "softening" law that monotonically decreases with  $\delta$ , energy analysis reveals that approach as unnecessarily restrictive. The only energy requirement is that  $d\Omega \geq 0$ . Thus any  $F(\delta)$  with  $\varphi(\delta) \geq 0$  is a possible strength model. Appendix I remarks on alternative, but identical, methods that either define  $F(D)$  strength models to postulate damage evolution in terms  $D$  instead of  $\delta$ .

## 2.2. Three Dimensional Damage Mechanics

The most common approach to 3D damage mechanics is called isotropic or scalar damage mechanics. In brief, this method assumes the partitioning tensor is diagonal,  $\mathbf{D} = d\mathbf{I}$ , where  $d$  is a scalar damage parameter. The implementation then applies 1D methods, but replaces  $\varepsilon$  with an *effective* strain such that the failure surface becomes

$$\Phi(\boldsymbol{\sigma}, \delta) = E(1-d)\varepsilon_{eff} - F(\delta) \quad (10)$$

For example, Oliver suggests using  $\varepsilon_{eff} = \sqrt{\boldsymbol{\varepsilon} \cdot \mathbf{C}\boldsymbol{\varepsilon}}/E$  (scaled here by dividing by  $E$  to make  $\varepsilon_{eff}$  dimensionless) with  $F(\delta)$  defining an evolving 3D strength [14]. The 1D consistency analysis then easily extends to 3D evolution of

$$d\delta = \frac{\boldsymbol{\sigma} \cdot d\boldsymbol{\varepsilon}}{F(\delta)\left(1 + \frac{F'(\delta)}{E}\right)} \quad \text{and} \quad d(d) = \mathbb{R}(\delta)d\delta \quad (11)$$

When deriving damage mechanics to model cracks, however, this "isotropic" extension to 3D is unacceptable. Its main problem is choice of  $\mathbf{D} = d\mathbf{I}$ , which implies materials soften the same in all directions in response to damage. Isotropic softening works in 1D because there is only in one direction, but, in 3D a material should soften differently in different directions. Modeling this 3D response requires knowledge of crack orientation by its normal vector  $\hat{\mathbf{n}}$  and extension of both  $\mathbf{D}$  and  $\Phi(\boldsymbol{\sigma}, \delta, \dots)$  to explicitly depend on  $\hat{\mathbf{n}}$  and potentially more damage variables. Crack orientation is determined by postulating a damage initiation criterion that predicts both *when* damage initiates and *normal vector*  $\hat{\mathbf{n}}$  for that crack. Methods (and requirements) for choosing initiation criteria are discussed later; for now, we assume  $\hat{\mathbf{n}}$  is available to the damage analysis.

Once damage initiates and  $\hat{\mathbf{n}}$  is known, damage modeling is best done in a *crack axis system* (CAS) where crack normal is in the  $x$  direction or  $\hat{\mathbf{n}} = \hat{\mathbf{x}}$ . Imagine a cubical particle in the CAS with sides of length  $\Delta x$  that is deformed only by cracking strain. Inverting Eq. (3) when  $\hat{\mathbf{n}} = (1, 0, 0)$  and  $h = \Delta x$  relates crack opening displacement to cracking strain:

$$\mathbf{u}^{(COD)} = \Delta x (\varepsilon_{c,xx}, \gamma_{c,xy}, \gamma_{c,xz})$$

and shows that  $\varepsilon_{c,yy} = \varepsilon_{c,zz} = \gamma_{c,yz} = 0$ . These requirements mean that rows 2, 3, and 4 of  $\mathbf{D}$  must be zero (when expressing  $\mathbf{D}$  using Voigt notation with strains ordered  $\varepsilon_{xx}, \varepsilon_{yy}, \varepsilon_{zz}, \gamma_{yz}, \gamma_{xz}$ ,

and  $\gamma_{xy}$  in the CAS). For a generally anisotropic material (where all elements of  $\mathbf{C}$  may be nonzero), requiring  $\mathbf{C}(\mathbf{I}-\mathbf{D})$  to be symmetric gives 15 equations from the 15 off-diagonal elements to determine the 18 elements of  $\mathbf{D}$ . Assigning the three diagonal elements of  $\mathbf{D}$  to  $D_{11} = H(\sigma_{xx})d_n$ ,  $D_{55} = d_{xz}$ , and  $D_{66} = d_{xy}$ , where  $d_n$ ,  $d_{xy}$ , and  $d_{xz}$  are three damage state parameters and  $H(\sigma_{xx})$  is the Heaviside function to distinguish cracks in tension or compression, reduces to a linear equation for the 15 unknown elements of  $\mathbf{D}$ . Reference [10] raised a conjecture that a generally-anisotropic material should have

$$D_{ij} = \frac{C_{ij}d_j}{C_{jj}} \quad \text{with} \quad d_1 = H(\sigma_{xx})d_n, \quad d_5 = d_{xz}, \quad d_6 = d_{xy}, \quad d_2 = d_4 = d_3 = 0$$

While this conjecture does satisfy the linear system (and therefore  $\mathbf{C}(\mathbf{I}-\mathbf{D})$  is symmetric), the determinant of the matrix for determining  $\mathbf{D}$  is zero. In other words, proceeding for generally-anisotropic materials requires additional constraints for a unique solution. But, if analysis is limited to orthotropic materials and the response remains orthotropic after damage (but with altered properties), a unique solution for  $\mathbf{D}$  in 3D (which follows the Ref. [10] conjecture) is obtained:

$$\mathbf{D} = \begin{bmatrix} H(\sigma_{xx})d_n & \frac{H(\sigma_{xx})C_{12}}{C_{11}}d_n & \frac{H(\sigma_{xx})C_{13}}{C_{11}}d_n & 0 & 0 & 0 \\ 0 & 0 & 0 & 0 & 0 & 0 \\ 0 & 0 & 0 & 0 & 0 & 0 \\ 0 & 0 & 0 & 0 & d_{xz} & 0 \\ 0 & 0 & 0 & 0 & 0 & d_{xy} \end{bmatrix} \quad (12)$$

Note that crack opening in the normal direction is  $u_x^{(COD)} = \Delta x \varepsilon_{c,xx}$ . In compression,  $H(\sigma_{xx} < 0) = 0$ , which correctly leads to zero normal displacement. In tension,  $H(\sigma_{xx} > 0) = 1$  allows cracks to open. All subsequent equations assume orthotropic symmetry before damage and in the CAS after damage (i.e.,  $\hat{\mathbf{x}}$  in the CAS is in a damaged material symmetry direction).

This  $\mathbf{D}$  matches the damage tensor first proposed by Chaboche [2] (but here transposed and with the  $H(\sigma_{xx})$  modifications). A key difference is that Chaboche derived it as a *specific*  $\mathbf{D}$  based on a model for stiffness reduction due to an array of aligned microcracks. The strain-partitioning view of  $\mathbf{D}$  allows it to be derived without reference to stiffness reduction modeling. Furthermore, the strain-partitioning view asserts that  $\mathbf{D}$  is not a choice — it is the *only option* consistent with damage mechanics modeling a crack. As a consequence, isotropic damage mechanics using  $\mathbf{D} = d\mathbf{I}$  is inconsistent with a crack. Similarly, orthotropic damage mechanics with alternative  $\mathbf{D}$  tensors (e.g., [9]) are inconsistent with a crack (note when a model gives only  $\mathbf{C}_{eff}$  in the presence of damage, the  $\mathbf{D}$  tensor implied by that model is easily derived as  $\mathbf{D} = \mathbf{I} - \mathbf{C}_{eff}\mathbf{C}^{-1}$ ). I do not claim such prior work is useless or undeserving of being called “damage mechanics.” I do claim, however, that damage mechanics models of orthotropic materials with  $\mathbf{D}$  differing from Eq. (12) are classes of damage mechanics that are not modeling cracks. Such methods develop non-physical cracking strains that correspond to displacements not associated with a single crack opening displacement.

A second problem with both isotropic damage mechanics and prior orthotropic damage mechanics is use of inappropriate failure surfaces such as Eq. (10) (or any other scalar function of principal stresses or strains). Simple scalar functions of stress or strain are insufficient for 3D and unable to partition into tensile and shear failure. The preferred approach is to postulate a failure surface that depends on three components of the traction vector on the crack surface,  $\mathbf{T} = \boldsymbol{\sigma} \cdot \hat{\mathbf{n}}$ . During modeling in the CAS, this traction increments by  $d\mathbf{T} = (d\sigma_{xx}, d\tau_{xy}, d\tau_{xz})$ . Given a 3D stress increment allowing for changes in  $\mathbf{D}$ :

$$d\boldsymbol{\sigma} = \nabla \boldsymbol{\sigma} \cdot (d\boldsymbol{\varepsilon}, d\mathbf{D}) = \mathbf{C}(\mathbf{I}-\mathbf{D})d\boldsymbol{\varepsilon} - \mathbf{C}d\mathbf{D}\boldsymbol{\varepsilon}$$

and  $\mathbf{D}$  in Eq. (12), the traction increment is:

$$d\mathbf{T} = \begin{pmatrix} d\sigma_{xx} \\ d\tau_{xy} \\ d\tau_{xz} \end{pmatrix} = \begin{pmatrix} C_{11}(d\varepsilon_n - H(\sigma_{xx})d(d_n\varepsilon_n)) \\ C_{66}(d\gamma_{xy} - d(d_{xy}\gamma_{xy})) \\ C_{55}(d\gamma_{xz} - d(d_{xz}\gamma_{xz})) \end{pmatrix}$$

where

$$\varepsilon_n = \varepsilon_{xx} + \frac{C_{12}}{C_{11}}\varepsilon_{yy} + \frac{C_{13}}{C_{11}}\varepsilon_{zz}$$

is an effective strain normal to the crack.

We proceed by defining a traction failure surface that depends on  $\hat{\mathbf{n}}$  through  $\mathbf{T} = \boldsymbol{\sigma} \cdot \hat{\mathbf{n}}$ :

$$\Phi(\mathbf{T}, \mathbf{c}) = \|\mathbf{T}\| - S(\mathbf{c})$$

where  $\mathbf{c} = (\varepsilon_n, \gamma_{xy}, \gamma_{xz}, \delta_n, \delta_{xy}, \delta_{xz})$  is a vector of strains and three damage variables that are needed to extend damage mechanics to 3D.  $\delta_n$ ,  $\delta_{xy}$  and  $\delta_{xz}$ , correspond to the cracking strain required to initiate damage in the current damage state if unloaded and then reloaded by uniaxial normal or shear stress loading, respectively. Their relations to  $d_n$ ,  $d_{xy}$ , and  $d_{xz}$  are thus analogous to Eq. (4):

$$d_n = \frac{\delta_n}{\delta_n + \frac{F_n}{C_{11}}} \quad d_{xy} = \frac{\delta_{xy}}{\delta_{xy} + \frac{F_{xy}}{C_{66}}} \quad d_{xz} = \frac{\delta_{xz}}{\delta_{xz} + \frac{F_{xz}}{C_{55}}} \tag{13}$$

where  $F$  subscripts imply strength models that depend on  $\delta_n$ ,  $\delta_{xy}$ , or  $\delta_{xz}$  (this same convention is used below for  $\mathbb{R}(\delta)$  and  $\varphi(\delta)$  functions).  $S(\mathbf{c})$  is a strength model that gives maximum traction allowed on the crack surface. It must be a state function of damage that can be achieved by defining it in terms of three unidirectional strength models —  $F_n(\delta_n)$ ,  $F_{xy}(\delta_{xy})$ , and  $F_{xz}(\delta_{xz})$  — one for normal and two for shear failure. Strength may also depend on mode mixity, which means it may depend on relative strains,  $\varepsilon_n$ ,  $\gamma_{xy}$ , and  $\gamma_{xz}$ , but not on their magnitudes.

By logic in 1D modeling, given current 3D stress,  $\boldsymbol{\sigma}$ , and an increment in total strain,  $d\boldsymbol{\varepsilon}$ , calculate a trial crack traction update  $\mathbf{T}^{(trial)} = \mathbf{T} + d\mathbf{T}$  where  $d\mathbf{T}$  is found with constant  $d_n$ ,  $d_{xy}$ , and  $d_{xz}$ . If  $\Phi(\mathbf{T}^{(trial)}, \mathbf{c}) \leq 0$ , the increment is elastic. The stress updates by  $d\boldsymbol{\sigma} = \mathbf{C}(\mathbf{I} - \mathbf{D})d\boldsymbol{\varepsilon}$ , no changes are made to  $d_i$  or  $\delta_i$ , but current cracking strain changes by  $d\boldsymbol{\varepsilon}_c = \mathbf{D}d\boldsymbol{\varepsilon}$ . But, if  $\Phi(\mathbf{T}^{(trial)}, \mathbf{c}) > 0$ , damage evolves. The damage evolution can be determined from a 3D consistency condition:

$$\nabla\Phi(\mathbf{T}, \mathbf{c}) \cdot (d\boldsymbol{\varepsilon}, d\mathbf{c}) = 0 \quad \implies \quad \nabla\|\mathbf{T}\| \cdot (d\boldsymbol{\varepsilon}, d\mathbf{c}) = \nabla S(\mathbf{c}) \cdot d\mathbf{c} \tag{14}$$

Further results depend on choice for  $S(\mathbf{c})$ . First, however, note that this analysis provides a single equation while the update has three unknown damage increments:  $d\delta_n$ ,  $d\delta_{xy}$  and  $d\delta_{xz}$ . Some prior ADaM models have proposed coupling between damage variables [2]. This analysis proposes that coupling should be determined by requiring all components of crack traction to simultaneously decay to zero at failure. The details depend on choice  $S(\mathbf{c})$ , which can be represented in a 3D plot with crack tractions  $\sigma_{xx}$ ,  $\tau_{xy}$ , and  $\tau_{xz}$  along the  $x$ ,  $y$ , and  $z$  axes, respectively. The following sections consider the three failure surfaces in Fig. 2.

**2.2.1. Cuboid Strength Model:** The simplest strength model is an open-ended cuboid surface (see Fig. 2A) intersecting the  $y$  axis at  $\pm F_{xy}$ , the  $z$  axis at  $\pm F_{xz}$ , and the positive  $x$  axis at  $F_n$ . The compression end (negative  $x$  axis) is unbounded or failure in compression happens only by shear. One approach to a cuboid strength model is to allow the three damage variables to evolve independently whenever any crack traction component reaches strength in that direction. This surface thus leads to three uncoupled 1D damage increments all based on Eq. (7):

$$d\delta_n = \frac{d\varepsilon_n}{1 + \frac{F'_n}{C_{11}}} \quad d\delta_{xy} = \frac{\text{sign}(\tau_{xy})d\gamma_{xy}}{1 + \frac{F'_{xy}}{C_{66}}} \quad \text{and} \quad d\delta_{xz} = \frac{\text{sign}(\tau_{xz})d\gamma_{xz}}{1 + \frac{F'_{xz}}{C_{55}}} \tag{15}$$

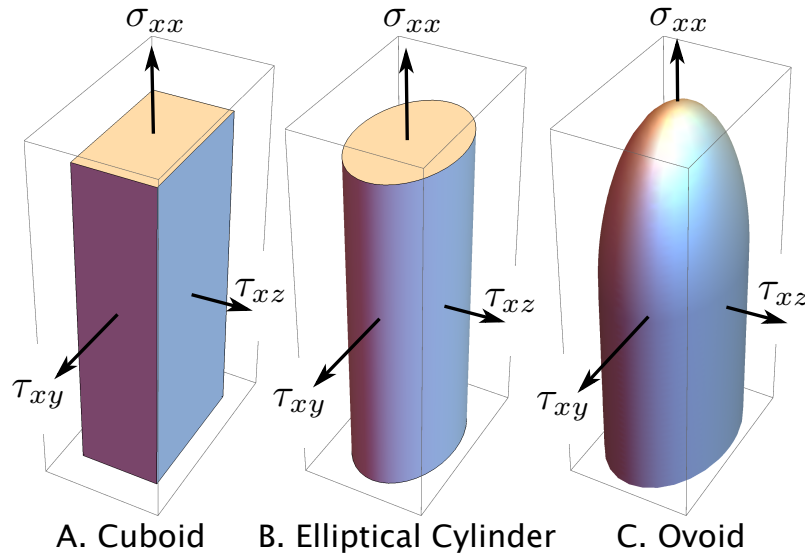


Figure 2. Plots for three strength models,  $S(c)$ , based on A. a cuboid surface, B. an elliptical cylinder surface, and C. an ovoid surface. The  $x$  direction is the normal strength while the  $y$  and  $z$  directions are the shear strengths.

The shear evolutions are modified with  $\text{sign}(\tau_{ij}) = \tau_{ij}/|\tau_{ij}|$  to allow damage evolution by positive or negative shear. The cracking strain increments are  $d\varepsilon_{c,xx} = d\delta_n$  and  $d\gamma_{c,ij} = \text{sign}(\tau_{ij})d\delta_{ij}$ .

This option provides an “uncoupled” approach. It is identical to ADaM implementation in Ref. [10] and similar to uncoupled methods used in cohesive zone modeling of mixed-mode failures [17]. A drawback of uncoupled methods is they result in unrealistic modeling of damage effects. Imagine loading a material in tension to induce normal damage causing an increase in  $d_n$  and  $\delta_n$ . If this material was then unloaded and reloaded in shear, it would act as a virgin material with no damage.

More realistic modeling should allow for damage in one direction to affect subsequent deformation in other directions [18]. A extension for a cuboid surface that achieves this goal is to link the damage state parameters or to set  $d_n = d_{xy} = d_{xz} = d$ . Although this approach appears to be an *ad hoc* assumption, it has physical justification by resulting in all components of crack traction simultaneously reaching zero at failure. Implementation of this coupling repeats the three calculations in Eq. (15), but the linked  $d$  parameter updates by the one that changes the most:

$$d(d) = \max(\mathbb{R}_n d\delta_n, \mathbb{R}_{xy} d\delta_{xy}, \mathbb{R}_{xz} d\delta_{xz})$$

Given this update and one direction that provides the maximum change, the other two  $\delta$  parameters are updated by inverting Eq. (13) (e.g.,  $\delta_n + d\delta_n = \delta_n^{-1}(d + d(d))$ ). Increments in cracking strains during coupled, 3D damage evolution are found from:

$$d\varepsilon_{c,xx} = d(d\varepsilon_n) = d d\varepsilon_n + \varepsilon_n \mathbb{R}_n d\delta_n = d d\varepsilon_n + \frac{\sigma_{xx} d\varphi_n}{C_{11} \delta_n F_n} d\delta_n$$

This increment can be transformed to

$$d\varepsilon_{c,xx} = \frac{\sigma_{xx}}{F_n} d\delta_n + d \left( d\varepsilon_n - \frac{\sigma_{xx}}{F_n} \left( 1 + \frac{F'_n}{C_{11}} \right) d\delta_n \right) \tag{16}$$

Analogous equations apply for  $d\gamma_{c,xy}$  and  $d\gamma_{c,xz}$ . Notice that the direction that maximizes  $d(d)$  will update as in 1D damage mechanics. For example, if the controlling direction is the  $n$  direction, then  $\sigma_{xx} = F_n$ ,  $1 + F'/C_{11} = d\varepsilon_n/d\delta_n$  and the update simplifies to  $d\varepsilon_{c,xx} = d\delta_n$ .

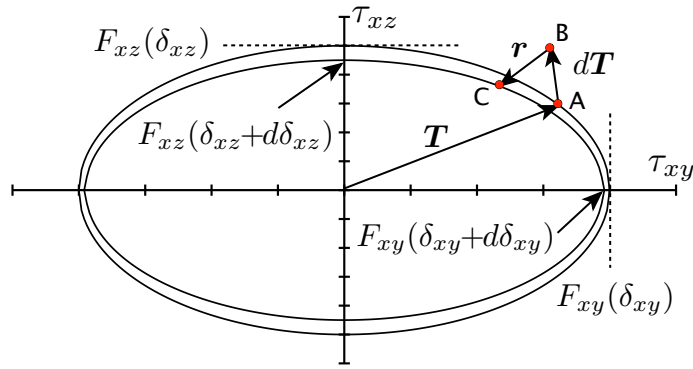


Figure 3. Cross section of an elliptical cylinder failure surface for analyzing damage evolution in shear.  $T$  is an initial traction to point A. Point B is a trial traction that causes damage. Point C is final traction after returning to an evolved failure surface.  $F_{ij}(\delta_{ij})$  and  $F_{ij}(\delta_{ij} + d\delta_{ij})$  indicate initial and evolved strengths in the two shear directions.

The two other directions, however, need the full Eq. (16). Thus, unlike 1D, where  $\delta$  equals the maximum cracking strain,  $\delta_n$ ,  $\delta_{xy}$  and  $\delta_{xz}$  are, in general, *not equal* to maximum normal and shear cracking strains.

2.2.2. *Elliptical Cylinder Strength Model:* This surface is an elliptical cylinder that is capped on the top at  $F_n$  and open-ended on the bottom (see Fig. 2B). Starting with uncoupled tension and shear, normal damage evolution uses the cuboid method in Eq. (15) while the shear strength evolves to an elliptical cross-section of the cylinder that intersects the  $y$  axis at  $\pm F_{xy}$  and the  $z$  axis at  $\pm F_{xz}$  (see Fig. 3).

For  $S(c)$ , we write shear traction magnitude  $T_s = (\tau_{xy}, \tau_{xz})$ , in terms of damage parameters:

$$\|T_s\| = \|\gamma\| \sqrt{C_{66}^2(1 - d_{xy})^2 \sin^2 \theta + C_{55}^2(1 - d_{xz})^2 \cos^2 \theta} = k_s \|\gamma\|$$

where  $\gamma = (\gamma_{xy}, \gamma_{xz}) = \|\gamma\|(\sin \theta, \cos \theta)$ ,  $\|\gamma\| = \sqrt{\gamma_{xy}^2 + \gamma_{xz}^2}$ ,  $\tan \theta = \gamma_{xy} / \gamma_{xz}$ , and

$$k_s = \sqrt{C_{66}^2(1 - d_{xy})^2 \sin^2 \theta + C_{55}^2(1 - d_{xz})^2 \cos^2 \theta}$$

is current shear stiffness or slope of  $\|T_s\|$  vs.  $\|\gamma\|$ . This traction magnitude causes damage when it reaches the elliptical surface, or when

$$1 = \left(\frac{\tau_{xy}}{F_{xy}}\right)^2 + \left(\frac{\tau_{xz}}{F_{xz}}\right)^2 = \|\gamma_d\|^2 \left(\frac{C_{66}^2(1 - d_{xy})^2 \sin^2 \theta}{F_{xy}^2} + \frac{C_{55}^2(1 - d_{xz})^2 \cos^2 \theta}{F_{xz}^2}\right)$$

where  $\gamma_d$  is shear strain vector when the traction vector is on the traction failure surface. Solving for its magnitude gives:

$$\|\gamma_d\| = \frac{F_{xy}F_{xz}}{\sqrt{F_{xz}^2 C_{66}^2(1 - d_{xy})^2 \sin^2 \theta + F_{xy}^2 C_{55}^2(1 - d_{xz})^2 \cos^2 \theta}}$$

The traction failure surface can now be represented by a 4D surface:

$$S(\theta, \delta_{xy}, \delta_{xz}) = k_s \|\gamma_d\| = F_{xy}F_{xz} \sqrt{\frac{C_{66}^2(1 - d_{xy})^2 \sin^2 \theta + C_{55}^2(1 - d_{xz})^2 \cos^2 \theta}{F_{xz}^2 C_{66}^2(1 - d_{xy})^2 \sin^2 \theta + F_{xy}^2 C_{55}^2(1 - d_{xz})^2 \cos^2 \theta}}$$

The damage evolution equation becomes:

$$\nabla\Phi(\mathbf{T}, \mathbf{c}) \cdot (d\boldsymbol{\varepsilon}, d\mathbf{c}) = \nabla(\|\mathbf{T}_s\| - S(\theta, \delta_{xy}, \delta_{xz})) \cdot (d\gamma_{xy}, d\gamma_{xz}, d\delta_{xy}, d\delta_{xz}) = 0 \quad (17)$$

After a tedious derivation, this equation simplifies to a useful result, but the same result can be found by a much simpler path. Figure 3 shows initial traction  $A$  on the initial failure surface while  $B$  is a trial traction found by assuming no damage evolution:

$$B = (\tau_{xy}^{(trial)}, \tau_{xz}^{(trial)}) = (\tau_{xy} + C_{66}(1 - d_{xy})d\gamma_{xy}, \tau_{xz} + C_{55}(1 - d_{xz})d\gamma_{xz})$$

When  $B$  is outside the surface, we must return to  $C$  on an evolved surface, which in terms of unknown increments  $d\delta_{xy}$  and  $d\delta_{xz}$  is:

$$C = (\tau_{xy}^{(final)}, \tau_{xz}^{(final)}) = (\tau_{xy}^{(trial)} - C_{66}\gamma_{xy}\mathbb{R}_{xy}d\delta_{xy}, \tau_{xz}^{(trial)} - C_{55}\gamma_{xz}\mathbb{R}_{xz}d\delta_{xz}) = B - \mathbf{r}$$

where  $\mathbf{r} = (C_{66}\gamma_{xy}\mathbb{R}_{xy}d\delta_{xy}, C_{55}\gamma_{xz}\mathbb{R}_{xz}d\delta_{xz})$  is the “return” vector in the  $y$ - $z$  plane. The damage evolution equation can be derived by finding increments such that updated state is on the evolved elliptical surface or:

$$\left(\frac{\tau_{xy}^{(trial)} - r_y}{F_{xy}(\delta_{xy} + d\delta_{xy})}\right)^2 + \left(\frac{\tau_{xz}^{(trial)} - r_z}{F_{xz}(\delta_{xz} + d\delta_{xz})}\right)^2 = 1 \quad (18)$$

Expanding this equation in a multidimensional Taylor series and keeping only first-order terms in  $d\gamma_{xy}$ ,  $d\gamma_{xz}$ ,  $d\delta_{xy}$ , and  $d\delta_{xz}$ , the evolution equation simplifies to:

$$\begin{aligned} & \frac{\tau_{xy}^2 C_{66}(1 - d_{xy})\left(1 + \frac{F'_{xy}}{C_{66}}\right)}{F_{xy}^3} d\delta_{xy} + \frac{\tau_{xz}^2 C_{55}(1 - d_{xz})\left(1 + \frac{F'_{xz}}{C_{55}}\right)}{F_{xz}^3} d\delta_{xz} \\ & = \frac{\tau_{xy} C_{66}(1 - d_{xy})}{F_{xy}^2} d\gamma_{xy} + \frac{\tau_{xz} C_{55}(1 - d_{xz})}{F_{xz}^2} d\gamma_{xz} \end{aligned} \quad (19)$$

This results matches a tedious derivation using Eq. (17) and is a new result in ADaM.

To complete shear coupling, we need a second equation in damage increments. As done to couple cubic surface updates, the two shear damage parameter can be assumed to be linked such that  $d_{xy} = d_{xz} = d_s$ . Adopting this linkage, the second equation is  $\mathbb{R}_{xy}d\delta_{xy} = \mathbb{R}_{xz}d\delta_{xz}$ . Substitution into Eq. (19) gives damage increments of

$$d(d_s) = \frac{\hat{\mathbf{T}}_e \cdot \left(\frac{C_{66}}{F_{xy}} d\gamma_{xy}, \frac{C_{55}}{F_{xz}} d\gamma_{xz}\right)}{\hat{\mathbf{T}}_e \cdot \left(\frac{\hat{\mathbf{T}}_{c,x} C_{66}}{\mathbb{R}_{xy} F_{xy}} \left(1 + \frac{F'_{xy}}{C_{66}}\right), \frac{\hat{\mathbf{T}}_{c,y} C_{55}}{\mathbb{R}_{xz} F_{xz}} \left(1 + \frac{F'_{xz}}{C_{55}}\right)\right)} \quad \text{with} \quad \hat{\mathbf{T}}_e = \left(\frac{\tau_{xy}}{F_{xy}}, \frac{\tau_{xz}}{F_{xz}}\right) \quad (20)$$

is a unit vector defined by the elliptical failure surface. The  $\delta$  damage variables evolve by  $d\delta_{ij} = d(d_s)/\mathbb{R}_{ij}$ . Besides just asserting that  $d_{xy} = d_{xz}$ , various physical justifications for coupling were explored. As described in Appendix II, equating damage parameters is the preferred approach and physically corresponds to returning to the evolved surface in the direction of the origin (*i.e.*, parallel to the traction vector).

As in coupling for the cubic traction surface, the shear cracking strain updates must use the general analysis in Eq. (16), which for shear becomes:

$$d\gamma_{c,xy} = \frac{\tau_{xy}}{F_{xy}} d\delta_{xy} + d_s \left( d\gamma_{xy} - \frac{\tau_{xy}}{F_{xy}} \left(1 + \frac{F'_{xy}}{C_{66}}\right) d\delta_{xy} \right) \quad (21)$$

with a corresponding result for  $d\gamma_{c,xz}$ . Because 3D damage may occur when  $\delta_{xy} \neq \gamma_{c,xz}$ ,  $\delta_{xy}$  no longer corresponds to the *maximum cracking strain*. It still, however, does correspond to the *cracking strain* required to cause damage if unloaded and then reloaded by only  $\tau_{xy}$ .

For an isotropic material,  $F_{xy} = F_{xz} = F_s$ ,  $\delta_{xy} = \delta_{xz} = \delta_s$ ,  $\mathbb{R}_{xy} = \mathbb{R}_{xz} = \mathbb{R}_s$ ,  $C_{55} = C_{66} = G$ , and  $\hat{T}_s = F_s \hat{T}_e$  is a unit vector in the shear traction direction. Noting that  $\|\mathbf{T}_s\| = F_s$  during damage evolution, the updates simplify to:

$$d\delta_s = \frac{\hat{T}_s \cdot d\boldsymbol{\gamma}}{1 + \frac{F'_s}{G}} \quad \text{and} \quad (d\gamma_{c,xy}, d\gamma_{c,xz}) = d\boldsymbol{\gamma}_c = \hat{T}_s d\delta_s + d_s (d\boldsymbol{\gamma} - \hat{T}_s (\hat{T}_s \cdot d\boldsymbol{\gamma})) \quad (22)$$

Updating normal damage by Eq. (15) and shear damage by Eq. (20) is a partially coupled analysis. The shear directions are coupled, but tension and shear directions are uncoupled. As a result, damage induced in tension would not affect subsequent loading in shear (and *vice versa*). As for the cubic surface, the coupling can be completed by linking  $d_n = d_s = d$ . Implementation of this approach would update by whether tensile or shear loading causes the most damage:

$$d(d) = \max(\mathbb{R}_n d\delta_n, d(d_s))$$

Normal and shear cracking strains then update by general results in Eqs. (16) and (21).

**2.2.3. Ovoid Strength Model:** An ovoid failure surface (see Fig. 2C) caps an open-ended elliptical cylinder in the compression half plane with an ovoid surface in the tensile half plane capped at  $F_n$ . The ovoid results can be derived from elliptical cylinder methods by adding terms corresponding to plotting  $\sigma_{xx}$  along the  $x$  axis of the traction failure surface plot. This extension adds:

$$\left( \frac{\sigma_{xx}^{(trial)} - r_x}{F_n(\delta_n + d\delta_n)} \right)^2 \quad \text{where} \quad r_x = C_{11}\epsilon_n \mathbb{R}_n d\delta_n$$

to Eq. (18). This extra term adds corresponding terms to left and right of Eq. (19). Finally, asserting this surface couples the three damage parameters ( $d = d_n = d_{xy} = d_{xz}$ ), the damage update, which is another new result in ADaM, becomes:

$$d(d) = \mathbb{R}_n d\delta_n = \frac{\hat{T}_o \cdot \left( \frac{C_{11}}{F_n} d\epsilon_n, \frac{C_{66}}{F_{xy}} d\gamma_{xy}, \frac{C_{55}}{\tau_{xz}} d\gamma_{xz} \right)}{\hat{T}_o \cdot \left( \frac{\hat{T}_{o,x} C_{11}}{\mathbb{R}_n F_n} \left( 1 + \frac{F'_n}{C_{11}} \right), \frac{\hat{T}_{o,y} C_{66}}{\mathbb{R}_{xy} F_{xy}} \left( 1 + \frac{F'_{xy}}{C_{66}} \right), \frac{\hat{T}_{o,z} C_{55}}{\mathbb{R}_{xz} F_{xz}} \left( 1 + \frac{F'_{xz}}{C_{55}} \right) \right)} \quad (23)$$

where  $\hat{T}_o = \left( \frac{\sigma_{xx}}{F_n}, \frac{\tau_{xy}}{F_{xy}}, \frac{\tau_{xz}}{F_{xz}} \right)$

is a unit vector defined by the ovoid failure surface. Shear damage increments by  $d\delta_{ij} = d(d)/\mathbb{R}_{ij}$ . The cracking strains increment by general results in Eqs. (16) and (21). For an isotropic material, this increment simplifies to

$$d(d) = \frac{\frac{\hat{T}_{o,x} C_{11}}{F_n} d\epsilon_n + \frac{G}{F_s} (\hat{T}_{o,y}, \hat{T}_{o,z}) \cdot d\boldsymbol{\gamma}}{\frac{\hat{T}_{o,x}^2 C_{11}}{\mathbb{R}_n F_n} \left( 1 + \frac{F'_n}{C_{11}} \right) + \frac{(\hat{T}_{o,y}^2 + \hat{T}_{o,z}^2) G}{\mathbb{R}_s F_s} \left( 1 + \frac{F'_s}{G} \right)} \quad (24)$$

In compression, where  $H(\sigma_{xx}) = 0$ , the normal stress terms drop out and the update reverts to elliptical cylinder methods in the previous section. But, because the  $d$  parameters remain linked even in compression, the normal damage variable update is  $d\delta_n = d(d)/\mathbb{R}_n$ . This damage increment, however, does not increment normal cracking strain — that strain remains zero in compression because of the  $H(\sigma_{xx})$  terms in **D**.

Finally, note that an ovoid surface with linked damage parameters inherently couples all damage variables. Unlike for cubic or elliptical cylinder surface, the implementation does not need to determine which direction causes the most damage.

2.2.4. *Energy Dissipation and Failure:* By Eq. (8), the energy dissipation rate with general  $\mathbf{D}$  simplifies to:

$$d\Omega = \frac{1}{2}H(\sigma_{xx})C_{11}\varepsilon_n^2 dd_n + \frac{1}{2}C_{55}\gamma_{xz}^2 dd_{xz} + \frac{1}{2}C_{66}\gamma_{xy}^2 dd_{xy}$$

In terms of  $\delta$  variables, the dissipation rate is:

$$d\Omega = \frac{1}{2}H(\sigma_{xx})\hat{T}_{0,x}^2 \varphi_n d\delta_n + \frac{1}{2}\hat{T}_{0,y}^2 \varphi_{xy} d\delta_{xy} + \frac{1}{2}\hat{T}_{0,z}^2 \varphi_{xz} d\delta_{xz}$$

This  $d\Omega$  differs from 1D energy dissipation in Eq. (9) by needing to account for damage occurring when  $\hat{T}_{0,i} < 1$  (i.e., current stress is below uniaxial strength in that direction). Note that dissipated energy partitions into tensile energy (the first term) and shear energy (the second two terms). The tensile energy is mode I fracture energy. The shear terms are a sum of mode II and mode III energy. These two shear modes cannot be separated because that separation requires evaluating deformation relative to the crack front. A smeared crack in a discrete volume element does not have a crack front.

When  $d$  damage parameters are linked, dissipation becomes:

$$d\Omega = \frac{1}{2} \left( H(\sigma_{xx})C_{11}\varepsilon_n^2 + C_{55}\gamma_{xz}^2 + C_{66}\gamma_{yz}^2 \right) d(d)$$

But, when using uncoupled damage parameters, dissipation is a sum of uncoupled dissipation terms. For example, an uncoupled cubic surface simplifies to  $d\Omega = d\bar{G}_n + d\bar{G}_{xy} + d\bar{G}_{xz}$  where increments are given by  $d\bar{G} = \varphi d\delta/2$  whenever any direction evolves damage. To model mixed-mode failure, a uncoupled cuboid surface must be supplemented with a failure criterion such as failure when

$$\left( \frac{\bar{G}_n}{\bar{G}_{n,c}} \right)^n + \left( \frac{\bar{G}_{xy}}{\bar{G}_{xy,c}} \right)^m + \left( \frac{\bar{G}_{xz}}{\bar{G}_{xz,c}} \right)^p = 1$$

where denominators are toughnesses in those directions and  $n$ ,  $m$ , and  $p$  would be material properties. A drawback of uncoupled modeling is that mixed-mode failure may occur when current tractions are non-zero. A sudden drop of all tractions to zero might cause numerical problems and may be a poor description of failure.

Coupled modeling with linked damage parameters has the desirable property that all tractions simultaneously decrease to zero at failure (i.e., when  $d \rightarrow 1$ ) and this failure occurs automatically without needing a mixed-mode failure criterion. This absence of a mixed-mode failure criterion might appear as a disadvantage to those interested in inputting mixed-mode failure properties, but it is actually a profound advantage. Stated differently, uncoupled methods must speculate and impose some mixed-mode failure criterion. In contrast, fully-coupled methods need no criterion; they automatically handle mixed-mode failure as a natural consequence of the chosen strength models. The effect of strength models on mixed-mode failure could be investigated by mixed-mode loading simulations. Favorable comparisons of such simulations to experimental mixed-mode failure observations could justify strength model selections.

2.2.5. *Post-Failure Contact and Friction:* Once failure occurs, the post-failure damage state uses  $d_n = d_{xy} = d_{xz} = 1$  and subsequent updates use the strain-partitioning interpretation of  $\mathbf{D}$  to update cracking strain by  $d\boldsymbol{\varepsilon}_c = \mathbf{D}d\boldsymbol{\varepsilon}$ . Such updates may result in large crack openings or in crack closing leading to crack-surface contact. Continued tracking of cracking strain automatically handles frictionless contact by the  $H(\sigma_{xx})$  terms in  $\mathbf{D}$  such that normal direction develops normal traction when in contact, but is stress free when opened while shear tractions are always zero. This frictionless contact is described in Ref. [10]; here contact is extended to model friction.

For a post-failure update when in contact, first assume the surfaces are sticking and calculate a trial shear traction based no change in cracking strains:

$$\mathbf{T}_s^{(trial)} = (\tau_{xy} + C_{66}d\gamma_{xy}, \tau_{xz} + C_{55}d\gamma_{xz})$$

If  $\|T_s^{(trial)}\| \leq \mu N$  (where  $N = -\sigma_{xx}$  is the surface compression), the crack plane sticks, accept the trial update in shear stress, and set increments in cracking strain to zero. But, if  $\|T_s^{(trial)}\| > \mu N$ , revise the shear stresses to:

$$T_s^{(final)} = (\tau_{xy} + \zeta C_{66} d\gamma_{xy}, \tau_{xz} + \zeta C_{55} d\gamma_{xz})$$

where  $\zeta$  is found by solving the quadratic equation  $\|T_s^{(final)}\|^2 = \mu^2 N^2$ . Once  $\zeta$  is found, the shear stresses are set to  $T_s^{(final)}$  and the cracking strain increments become:

$$(d\gamma_{c,xy}, d\gamma_{c,xz}) = (1 - \zeta)(d\gamma_{xy}, d\gamma_{xz})$$

Physically,  $\zeta = 0$  is frictionless while  $0 < \zeta \leq 1$  is modeling Coulomb friction. Frictional work per unit volume is shear force  $\times$  shear strain increment. Multiplying by particle volume  $V$ , the total frictional work is

$$W_F = \mu N V \sqrt{d\gamma_{c,xy}^2 + d\gamma_{c,xz}^2}$$

Converting this work into heat can model frictional heating.

### 3. GENERAL THEORY OF DAMAGE MECHANICS

The special theory assumes traction failure surfaces depend only on damage state. Real material strength often depends on other variables such as pressure, temperature, strain rate, or more. A general theory to account for other variables must change strength models to  $F(\delta, \alpha)$  where  $\alpha$  is a vector of all external variables affecting the material's strength. This change has two consequences. First, the ratio of  $D$  evolution to  $\delta$  evolution needs a full differential to account for  $\alpha$  dependence:

$$D = \frac{\delta}{\delta + \frac{F(\delta, \alpha)}{E}} \implies dD = \left(\frac{\partial D}{\partial \delta}\right)_{\alpha} d\delta + \left(\frac{\partial D}{\partial \alpha}\right)_{\delta} \cdot d\alpha = \mathbb{R}d\delta - \mathbb{A} \cdot d\alpha$$

where

$$\mathbb{A}_i(\delta, \alpha) = -\left(\frac{\partial D}{\partial \alpha_i}\right)_{\delta, \alpha_{j \neq i}} = \frac{\psi(\delta, \alpha_i)}{E\left(\delta + \frac{F(\delta, \alpha)}{E}\right)^2} \quad \text{with} \quad \psi(\delta, \alpha_i) = \delta \left(\frac{\partial F(\delta, \alpha)}{\partial \alpha_i}\right)_{\delta, \alpha_{j \neq i}}$$

Second, gradients of strength models add  $\alpha$  terms:

$$\nabla F(\delta, \alpha) \cdot (d\delta, d\alpha) = F'(\delta, \alpha)d\delta + \sum_i \frac{\psi(\delta, \alpha_i)d\alpha_i}{\delta}$$

where  $F'(\delta, \alpha)$  now indicates the  $\delta$  partial derivative.

Imagine an elastic process with  $\epsilon \rightarrow \epsilon + d\epsilon$  and  $\alpha \rightarrow \alpha + d\alpha$  such that stress remains below the current traction failure surface. Because this process dissipates no energy, it requires  $dD = 0$ . Solving for  $dD = 0$  implies an "elastic" change in  $\delta$ , denoted by  $d\delta^{(e)}$ , as:

$$d\delta^{(e)} = \frac{\mathbb{A} \cdot d\alpha}{\mathbb{R}} = \frac{\sum_i \psi(\delta, \alpha_i)d\alpha_i}{\varphi(\delta, \alpha)}$$

In the special theory, neither  $D$  nor any  $\delta$  values change unless damage evolves. In other words, both are damage state variables. But, in the general theory,  $\delta$  variables may change when damage is not evolving and therefore only  $D$  remains as a damage state variable.

The need to sum over  $\psi(\delta, \alpha_i)$  can be avoided by recognizing  $d\delta^{(e)}$  is the increment in  $\delta$  required to keep  $D$  constant when  $\alpha \rightarrow \alpha + d\alpha$  or:

$$\frac{\delta}{\delta + \frac{F(\delta, \alpha)}{E}} = \frac{\delta + d\delta^{(e)}}{\delta + d\delta^{(e)} + \frac{F(\delta + d\delta^{(e)}, \alpha + d\alpha)}{E}}$$

Equating the left hand side to the current  $D$ , leads to:

$$d\delta^{(e)} = \delta + \frac{DF(\delta + d\delta^{(e)}, \boldsymbol{\alpha} + d\boldsymbol{\alpha})}{E(1 - D)} \tag{25}$$

This equation can be numerically solved for  $d\delta^{(e)}$  given any strength model and a finite change in  $\boldsymbol{\alpha}$  (a strength model linear in  $\delta$  has an analytical solution).

Given these  $d\delta^{(e)}$  relations, a general damage mechanics theory can be deduced from methods analogous to the special theory by replacing  $\mathbb{R}d\delta$  terms with  $\mathbb{R}(\delta, \boldsymbol{\alpha})(d\delta - d\delta^{(e)})$  and  $F'(\delta)d\delta$  with:

$$\nabla F(\delta, \boldsymbol{\alpha}) \cdot (d\delta, d\boldsymbol{\alpha}) = F'(\delta, \boldsymbol{\alpha})d\delta + \frac{\varphi(\delta, \boldsymbol{\alpha})}{\delta}d\delta^{(e)}$$

Some general theory methods along with quoted extensions of special theory results are given in this section.

Beginning with 1D damage evolution, such as normal direction for a cuboid surface, the special theory result in Eq. (5) changes to

$$d\delta_n = \frac{C_{11}(1 - d_n)d\varepsilon_n + \left(C_{11}\varepsilon_n\mathbb{R}_n - \frac{\varphi_n}{\delta_n}\right)d\delta_n^{(e)}}{C_{11}\varepsilon_n\mathbb{R}_n + F'_n}$$

where  $F_n$ ,  $\mathbb{R}_n$ , and  $\varphi_n$  depend on both  $\delta$  (as indicated by the subscript) and on  $\boldsymbol{\alpha}$ . Substituting  $C_{11}\varepsilon_n\mathbb{R}_n = d_n\varphi_n/\delta_n$  during uniaxial damage and expanding the  $\varphi_n$  terms simplifies to:

$$d\delta_n = d\delta_n^{(e)} + \frac{d\varepsilon_n - d\varepsilon_n^{(e)}}{1 + \frac{F'_n}{C_{11}}} \quad \text{where} \quad d\varepsilon_n^{(e)} = \frac{d\delta_n^{(e)}}{d_n} \tag{26}$$

This general theory result is equivalent to breaking the increment into two steps. First, deform elastically on the traction failure surface while maintaining constant  $d_n$  to reach updated traction for  $\delta_n \rightarrow \delta_n + d\delta_n^{(e)}$  and  $\boldsymbol{\alpha} \rightarrow \boldsymbol{\alpha} + d\boldsymbol{\alpha}$  corresponding to elastic strain increment,  $d\varepsilon_n^{(e)}$ , found by strain partitioning of  $d_n$ . Second, evolve damage at constant  $\boldsymbol{\alpha} + d\boldsymbol{\alpha}$  as in the special theory, but change the strain increment causing damage to  $d\varepsilon_n^* = d\varepsilon_n - d\varepsilon_n^{(e)}$ .

A general cracking strain increment follows Eq. (16), but replaces  $d\delta_n$  with  $d\delta_n - d\delta_n^{(e)}$ :

$$d\varepsilon_{c,xx} = \frac{\sigma_{xx}}{F_n}(d\delta_n - d\delta_n^{(e)}) + d_n \left[ d\varepsilon_n - \frac{\sigma_{xx}}{F_n} \left(1 + \frac{F'_n}{C_{11}}\right) (d\delta_n - d\delta_n^{(e)}) \right] \tag{27}$$

For uniaxial damage by Eq. (26), this general cracking strain increment simplifies to  $d\varepsilon_{c,n} = d\delta_n$  (i.e. the process associated with  $d\delta_n^{(e)}$  does not change  $d_n$  and therefore does not affect cracking strain). The general shear damage equations for a cuboid surface extend to:

$$d\delta_{xy} = d\delta_{xy}^{(e)} + \frac{\text{sign}(\tau_{xy})d\gamma_{xy} - \frac{d\delta_{xy}^{(e)}}{d_{xy}}}{1 + \frac{F'_{xy}}{C_{66}}} \quad \text{and} \quad d\delta_{xz} = d\delta_{xz}^{(e)} + \frac{\text{sign}(\tau_{xz})d\gamma_{xz} - \frac{d\delta_{xz}^{(e)}}{d_{xz}}}{1 + \frac{F'_{xz}}{C_{55}}}$$

with cracking strain increments  $d\gamma_{c,ij} = \text{sign}(\tau_{ij})d\delta_{ij}$ .

Similarly, general theory updates for elliptical and ovoid surfaces follow the special theory results in Eqs. (20) and (23) but replace  $d\delta_{ij}$  with  $d\delta_{ij} - d\delta_{ij}^{(e)}$ ,  $d\delta_n$  with  $d\delta_n - d\delta_n^{(e)}$ ,  $d\gamma_{ij}$  with  $d\gamma_{ij} - d\gamma_{ij}^{(e)}$ , and  $d\varepsilon_n$  with  $d\varepsilon_n - d\varepsilon_n^{(e)}$ . A change in 3D methods (vs. 1D methods) is to derive 3D strain increments for elastic motion on the failure surface:

$$\left(d\varepsilon_n^{(e)}, d\gamma_{xy}^{(e)}, d\gamma_{xz}^{(e)}\right) = \left(\hat{T}_{o,x} \frac{d\delta_n^{(e)}}{d}, \hat{T}_{o,y} \frac{d\delta_{xy}^{(e)}}{d}, \hat{T}_{o,z} \frac{d\delta_{xz}^{(e)}}{d}, \right) \tag{28}$$

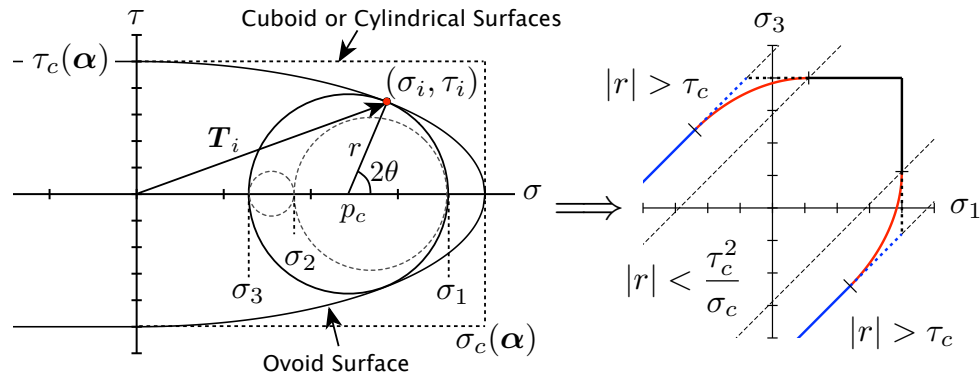


Figure 4. Damage initiation in an isotropic material based on Mohr's circles for principal stresses  $\sigma_1 \geq \sigma_2 \geq \sigma_3$  for each traction failure surface (ovoid: solid lines, cuboid and cylindrical: dotted lines).  $\sigma(\boldsymbol{\alpha})$  and  $\tau(\boldsymbol{\alpha})$  are  $\boldsymbol{\alpha}$ -dependent tensile and shear strengths. The right side plots initiation surface in principal stress space for  $\tau_c = 0.6\sigma_c$ . The dashed lines separate the three cases in Eq. (29).

Using Eq. (25), this elastic strain increment is easily verified to update an initial traction on the failure surface at  $\delta$  and  $\boldsymbol{\alpha}$  to a new state on that surface at  $\delta + d\delta^{(e)}$  and  $\boldsymbol{\alpha} \rightarrow \boldsymbol{\alpha} + d\boldsymbol{\alpha}$ . The updates for isotropic materials follow the special theory results in Eqs. (22) and (24) but replace  $d\delta_s$  with  $d\delta_s - d\delta_s^{(e)}$  and  $d\boldsymbol{\gamma}$  with  $d\boldsymbol{\gamma} - (d\boldsymbol{\gamma}_{xy}^{(e)}, d\boldsymbol{\gamma}_{xz}^{(e)})$ . Cracking strain increments use Eq. (27) for each strain component.

### 3.1. Damage Initiation

Some have suggested (including myself [10]) that various initiation criteria can be paired with various damage evolution methods. That suggestion is wrong. Instead, the initiation law *must be identical* to the postulated traction failure surface with the axes at  $F_n(0)$ ,  $F_{xy}(0)$ , and  $F_{xz}(0)$  (see Fig. 2). If they differ, the stress-strain curve would have a discontinuity between initiation, determined by initiation law, and post-failure deformation, determined by traction failure surface. A challenge when detecting initiation, however, is that crack normal is not yet defined. In brief, damage initiation must determine when traction along *any* normal in 3D space reaches a failure surface. When critical traction is first detected, the direction that was critical determines the crack normal. These calculations require all  $F(0)$  to be greater than zero and can be challenging for anisotropic materials. This section gives one method for isotropic materials.

Figure 4 plots a 3D stress state in a Mohr's stress plot where  $\sigma_1 \geq \sigma_2 \geq \sigma_3$  are the principal stresses. Next, superpose the traction failure surface as a function of normal and shear stress on a plane with normal stress along the  $x$  axis and shear stress along the  $y$  axis (a 2D plot suffices for isotropic materials). Initiation is detected by determining when a point on the largest Mohr's circle between  $\sigma_1$  and  $\sigma_3$  with radius equal to the maximum shear stress  $\tau_{max} = r = (\sigma_1 - \sigma_3)/2$  first contacts the traction failure surface.

First, consider cuboid and elliptical cylinder failure surfaces. In a Mohr's stress plot, these surfaces are open-ended rectangles indicated by the dotted lines in Fig. 4. Damage initiates if  $\sigma_1 = \sigma_c(\boldsymbol{\alpha})$  or if  $\tau_{max} = \tau_c(\boldsymbol{\alpha})$ . Initiation also needs the crack normal, which is determined by where the point intersects the failure surface. Failure by  $\sigma_1$  first touches the rectangle when  $\theta = 0$  or crack normal is in maximum principal stress direction. Failure by  $\tau_{max}$  intersects the surface when the crack normal is at  $45^\circ$  to the maximum principal stress direction. These two surfaces thus reduce to predicting initiation using principal stresses and their directions, which is a common method used in prior modeling [10]. A new assertion is that damage evolution based on cuboid or cylindrical failure surfaces *must* determine initiation by this principal stress approach. Notice this approach accommodates effects of  $\boldsymbol{\alpha}$  on strength by basing the rectangle on current strengths  $\sigma_c(\boldsymbol{\alpha})$  and  $\tau_c(\boldsymbol{\alpha})$ .

An ovoid failure surface (in tensile loading), plots as an ellipse with axes  $\tau_c(\boldsymbol{\alpha})$  and  $\sigma_c(\boldsymbol{\alpha})$  where we first assume  $\sigma_c(\boldsymbol{\alpha}) > \tau_c(\boldsymbol{\alpha})$ . The geometric problem is that given a circle of radius,  $r = \tau_{max}$ , find the critical circle midpoint,  $p_c$ , such that the circle first contacts the elliptical failure surface. If the current circle's center  $p = (\sigma_1 + \sigma_3)/2$  is greater than or equal to  $p_c$ , then damage initiates. This geometric problem has several solution methods [19]. One method is to solve for  $\tau_i$  on the ellipse as a function  $\sigma_i$  and substitute into the equation for a circle of radius  $r$  centered at  $p_c$  to derive a quadratic equation for  $\sigma_i$ :

$$\frac{c^2}{\sigma_c^2} \sigma_i^2 - 2p_c \sigma_i + (p_c^2 - r^2 + \tau_c^2) = 0$$

where  $c = \pm \sqrt{\sigma_c^2 - \tau_c^2}$  are the foci of the ellipse. For this equation to reduce to a single  $\sigma_i$  such that the circle touches the ellipse at a single point, its discriminant must be zero, which leads to:

$$p_c = \frac{c \sqrt{\tau_c^2 - r^2}}{\tau_c} \implies \left(\frac{p_c}{c}\right)^2 + \left(\frac{r}{\tau_c}\right)^2 = 1$$

But this analysis does not apply for all  $r$ . The two contact points for the circle at  $\pm 2\theta$  degenerate to a single point when the intersection is at the ellipse apex or when  $p_c + r = \sigma_c$ . This condition occurs when  $r < \tau_c^2/\sigma_c$ , or  $r$  is less than radius of curvature of the ellipse apex. The solution is also invalid for  $r > \tau_c$ . This limit corresponds to finding shear failure at  $\tau_{max} = \tau_c$ . In summary, damage initiation occurs by:

$$\text{initiation at } \begin{cases} p_c = \sigma_c - r & \text{for } r \leq \frac{\tau_c^2}{\sigma_c} \\ p_c = \frac{c}{\tau_c} \sqrt{\tau_c^2 - r^2} & \text{for } \frac{\tau_c^2}{\sigma_c} < r < \tau_c \\ r_c = \tau_c & \text{for } r \geq \tau_c \end{cases} \quad (29)$$

Damage initiation also needs the crack normal direction. For the first and last cases, the crack normal is  $\theta = 0^\circ$  or  $45^\circ$ , respectively (where  $\theta$  is rotation about the principal 2 axis). For the intermediate case, the angle is:

$$\theta = \frac{1}{2} \cos^{-1} \left( \frac{\tau_c}{cr} \sqrt{\tau_c^2 - r^2} \right) \quad (30)$$

The right side of Fig. 4 plots this initiation surface in principal stress space (a 2D surface or cross-section of a 3D surface). The first (tensile failure) and last (shear failure) cases in Eq. (29) are straight lines that are connected by the intermediate case with an elliptical curve tangent to the first and last cases. The crack angle,  $\theta$ , is angle between normal to this surface and the  $\sigma_1$  direction.

For materials with  $\tau_c(\boldsymbol{\alpha}) \geq \sigma_c(\boldsymbol{\alpha})$ , all circles with  $r < \tau_c$  also have  $r \leq \tau_c^2/\sigma_c$ , which eliminates the middle case. Thus, failure will be by shear if  $r \geq \tau_c$  or by tension if  $p \geq \sigma_c - r$  with crack normals at  $45^\circ$  or  $0^\circ$ , respectively. In other words, by the same criterion used for cuboid and cylindrical surfaces and shown by the dotted lines on the right side of Fig. 4.

#### 4. DISCUSSION WITH EXAMPLES

Providing compelling examples to demonstrate the validity of damage mechanics models is challenging. When applied to simple problems, such as uniaxial loading, many methods give satisfactory results. When applied to complex problems with unknown solutions, many damage mechanics methods (even misguided ones) may generate plausible, albeit different, results. Two good ways to evaluate damage mechanics are by soundness and completeness of the underlying theory and by experience in getting useful results in a variety of problems. This paper presents a complete theory that appears sound and my personal experience is that these

methods provide useful and stable results in many problems. This paper is restricted to some practical implementation details, one example illustrating differences between isotropic and anisotropic damage mechanics as well as coupled vs. uncoupled damage parameters, and two general-theory examples using pressure-dependent failure properties. A planned paper will provide more-detailed comparisons between various damage mechanics methods and fracture mechanics solutions. Finally, this section concludes with remarks about further implications of the strain-partitioning interpretation of  $\mathbf{D}$ .

#### 4.1. Implementation

All methods in this paper were implemented in particle-based, material point method (MPM) software [15]. Implementation details for uncoupled parameters are in Ref. [10]. This section covers changes needed to implement coupling by the ovoid failure surface and to implement general theory methods. Implementing coupling for cubic or elliptical cylinder surfaces would use similar methods. These details assume isotropic materials, but could be extended to anisotropic materials.

All particles (*i.e.*, material points) start undamaged with  $d = 0$  and  $\delta_n = \delta_s = 0$ . Initiation methods in Ref. [10] must change to the methods in the *Damage Initiation* section. After damage initiation, each time step is associated with an effective strain increment  $d\boldsymbol{\varepsilon} = (d\varepsilon_n, d\gamma_{xy}, d\gamma_{xz})$  and its associated  $\|\mathbf{T}^{(trial)}\|$ . When  $\Phi(\mathbf{T}^{(trial)}, \mathbf{c}) \leq 0$ , the update is elastic, but the new general methods must calculate elastic changes in  $\delta_n$  and  $\delta_s$  using Eq. (25). When  $\Phi(\mathbf{T}^{(trial)}, \mathbf{c}) > 0$ , general damage mechanics modeling divides each step into three sub-steps:

1. Move elastically at constant  $\boldsymbol{\alpha}$  until traction reaches the failure surface. Because any elastic sub-step path can be used, a stable approach is to move parallel to initial traction or to find  $d\mathbf{T} = \beta\mathbf{T}$  such that  $\Phi((1 + \beta)\mathbf{T}, \mathbf{c}) = 0$ . Solving for  $\beta$  and elastic strain to reach the surface ( $d\boldsymbol{\varepsilon}^{(1)}$ ) gives

$$\beta\|\mathbf{T}\| = \frac{F_n F_s}{\sqrt{F_s^2 \hat{T}_x^2 + F_n^2 (\hat{T}_y^2 + \hat{T}_z^2)}} - \|\mathbf{T}\| \quad d\boldsymbol{\varepsilon}^{(1)} = \frac{\beta\|\mathbf{T}\|}{1-d} \left( \frac{\hat{T}_x}{C_{11}}, \frac{\hat{T}_y}{G}, \frac{\hat{T}_z}{G} \right)$$

2. Move elastically along the traction failure surface (*i.e.*, at constant  $d$ ) to point where  $\boldsymbol{\alpha} \rightarrow \boldsymbol{\alpha} + d\boldsymbol{\alpha}$  and  $\boldsymbol{\delta} \rightarrow \boldsymbol{\delta} + d\boldsymbol{\delta}^{(e)}$  corresponding to strain increment  $d\boldsymbol{\varepsilon}^{(e)}$  in Eq. (28). Using Eq. (25), elastic strain increment for the first two sub-steps ( $d\boldsymbol{\varepsilon}^{(1*)} = d\boldsymbol{\varepsilon}^{(1)} + d\boldsymbol{\varepsilon}^{(e)}$ ) is

$$d\boldsymbol{\varepsilon}^{(1*)} = \frac{\|\mathbf{T}\|}{1-d} \left( \frac{\hat{T}_x}{C_{11}} \left( \frac{(1+\beta)F_n^*}{F_n} - 1 \right), \frac{\hat{T}_y}{G} \left( \frac{(1+\beta)F_s^*}{F_s} - 1 \right), \frac{\hat{T}_z}{G} \left( \frac{(1+\beta)F_s^*}{F_s} - 1 \right) \right)$$

where  $F^* = F(\boldsymbol{\delta} + d\boldsymbol{\delta}^{(e)}, \boldsymbol{\alpha} + d\boldsymbol{\alpha})$ .

3. Change the initial traction to  $\mathbf{T} + (1-d)(C_{11}, G, G)d\boldsymbol{\varepsilon}^{(1*)}$  and then evolve damage using the special theory but change the strain increment for that calculation to  $d\boldsymbol{\varepsilon}^{(2)} = d\boldsymbol{\varepsilon} - d\boldsymbol{\varepsilon}^{(1*)}$ . The total increment in damage variables includes both  $d\boldsymbol{\delta}$  from special-theory damage calculation and  $d\boldsymbol{\delta}^{(e)}$  from sub-step #2. The increments in cracking strain include both  $d * (d\boldsymbol{\varepsilon}^{(1)})$  from sub-step #1 and increments from this sub-step (by Eq. (27)).

Insuring stable calculations requires two details. First, the particle size must obey stability conditions derived in Ref. [10] or  $\Delta x_p < \min(\eta_n(K_{Ic}/\sigma_c)^2, \eta_s(K_{IIc}/\tau_c)^2)$  where  $\eta_n$  and  $\eta_s$  are factors that depend on  $F_n(\delta_n)$  and  $F_s(\delta_s)$  strength models (these factors are maximized at 2 for strength models linear in  $\delta$ ), and  $K_{Ic}$  and  $K_{IIc}$  are associated critical stress intensity toughnesses. When  $\sigma_c$ ,  $\tau_c$ ,  $K_{Ic}$  or  $K_{IIc}$  depend on  $\boldsymbol{\alpha}$ , maximum cell size should be based on the range in  $\boldsymbol{\alpha}$  expected during a simulation.

Although coupled damage mechanics has three damage variables ( $d$ ,  $\delta_n$ , and  $\delta_s$ ) that update at different rates, they are interrelated by Eq. (13). If each variable increments by explicit expressions for their updates, their values can drift from satisfying relations in Eq. (13). Because

$\mathbb{R}$  functions decay close to zero near decohesion, increments in  $\delta_n$  and  $\delta_s$  can become unstable (i.e., too “stiff”). The recommended, stable approach is to update the one variable that updates the least (relatively). For a given time step, fractional changes in damage variables are

$$\left( d(d), \frac{d\delta_n}{\delta_{n,max}}, \frac{d\delta_s}{\delta_{s,max}} \right) = d(d) \left( 1, \frac{1}{\mathbb{R}_n \delta_{n,max}}, \frac{1}{\mathbb{R}_s \delta_{s,max}} \right)$$

A stable update process is as follows: If  $\max(\mathbb{R}_n \delta_{n,max}, \mathbb{R}_s \delta_{s,max}) < 1$ , use the  $d(d)$  update equation. Otherwise, if  $\mathbb{R}_n \delta_{n,max} > \mathbb{R}_s \delta_{s,max}$  evaluate  $d\delta_n$  or else evaluate  $d\delta_s$ . Whichever increment is evaluated, calculate the other two using Eq. (13). For typical strength models, modeling starts by incrementing  $\delta_n$  or  $\delta_s$  but eventually shifts to incrementing  $d$  when approaching decohesion. Inverting Eq. (13) to find  $\delta$  from  $d$  may need numerical methods (an analytical inversion is available for strength models linear in  $\delta$ ).

To test for shear-locking effects seen in FEM, the patch test proposed by Cervera [8] was run in MPM modeling. In brief, this test loads a 100×200 mm specimen in tension past failure (with material properties  $E = 2000$  MPa,  $\nu = 0.3$ ,  $\sigma_c = 1$  MPa, and  $G_{Ic} = 250$  J/m<sup>2</sup>). An implementation fails this test if it develops any spurious shear or transverse normal stresses. An MPM implementation passes this test and thus appears to avoid shear locking effects. This result is not surprising because MPM and FEM implement material models differently. MPM basically implements continuum mechanics equations during the Lagrangian phase of each time step. That calculation is disconnected from the grid. The crack path in this patch test consisted of two rows of failed particles resulting in a cracked region filling one background grid cell (i.e., a model with two particles per cell in each direction). Such a crack path resolves a crack well when using standard linear shape functions [20]. But if linear shape functions are replaced by quadratic splines [21], two rows of particles are not enough to resolve a crack. This issue is a discretization issue of modeling a sharp change in properties and not issue inherent to ADaM. Fortunately, spline functions usually spread out the damage resulting in improved results vs. linear functions. Absence of shear locking in MPM is an advantage over FEM, but does not imply MPM implementation is free of challenges. The *Additional Options* section discussions some of those challenges with potential solutions.

#### 4.2. Isotropic vs. Anisotropic Damage Mechanics and Coupled vs. Uncoupled Damage Parameters

An example that illustrates differences between isotropic and anisotropic damage mechanics and between coupled and uncoupled damage parameters is uniaxial tension while varying  $f = \tau_c/\sigma_c$ . By Eqs. (29) and (30) the initiation stress and crack angle using the ovoid surface are

$$\sigma_i = \begin{cases} 2\tau_c f \sqrt{1-f^2} & f < \frac{1}{\sqrt{2}} \\ \sigma_c & f \geq \frac{1}{\sqrt{2}} \end{cases} \quad \text{and} \quad \theta = \begin{cases} \frac{1}{2} \cos^{-1} \left( \frac{f^2}{1-f^2} \right) & f < \frac{1}{\sqrt{2}} \\ 0 & f \geq \frac{1}{\sqrt{2}} \end{cases} \quad (31)$$

For cuboid or elliptical surfaces, which are equivalent in 2D, the initiation stress and angle for  $f < 1/2$  are  $\sigma_i = 2\tau_c f$  and  $\theta = \pi/4$  but changes for  $f \geq 1/2$  to  $\sigma_i = \sigma_c$  and  $\theta = 0$ . For isotropic damage mechanics using  $\varepsilon_{eff} = \sqrt{\boldsymbol{\varepsilon} \cdot \mathbf{C} \boldsymbol{\varepsilon}}/E$  with evolution by Eq. (11), initiation occurs when  $\sigma_i = \sigma_c$  (3D or plane stress) but changes to  $\sigma_i = \sigma_c/\sqrt{1-\nu^2}$  for plane strain. This “isotropic” initiation is independent of  $f$  and does not define a crack normal direction. Notice that because isotropic damage mechanics depends on all components of stress, it non-physically depends on out-of-plane  $\sigma_{zz}$  stress in plane strain rather than just depending on crack traction. Isotropic damage mechanics could be improved by changing the failure surface, but it would still depend on inappropriate stress components and still unrealistically soften isotropically after initiation.

To compare approaches, a 42×6 mm bar was loaded in plane strain MPM. The material properties were  $E = 1000$  MPa,  $\nu = 0.33$ ,  $\rho = 1$  g/cm<sup>3</sup>,  $G_{Ic} = 1000$  J/m<sup>2</sup>,  $G_{IIc} = 4000$  J/m<sup>2</sup>, and  $\sigma_c = 15$  MPa. The bar was loaded at 2 m/s (or 0.2% of the material’s wave speed) using 0.33 mm cells in the background grid and  $f$  was varied from 0.1 to 1.0. The strength models were linear.

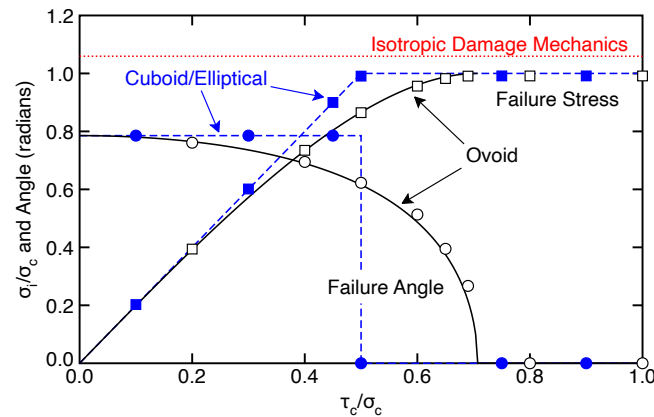


Figure 5. The load at initiation of failure ( $\sigma_i$  normalized to  $\sigma_c$ , square symbols) and angle of the initiated failure plane (in radians, circle symbols) as a function of  $f = \tau_c/\sigma_c$  for axial loading of a bar. The solid and dashed lines are expected results based on principal-stress initiation criteria for coupled and uncoupled methods, respectively.

Figure 5 compares simulations using ovoid surface (open symbols) or cuboid/elliptical surfaces (filled symbols) to corresponding initiation predictions (solid and dashed lines) as a function for  $f$ . The results match expectations. A benefit of an ovoid surface is that it provides a smooth transition in failure load and angle as  $f$  decreases. Cuboid/elliptical surfaces have a sharp jump in failure angle at  $f = 1/2$ . The results for isotropic damage mechanics matched the plane-strain initiation stress (dotted line), which is independent of  $f$  and provided no information about failure angle.

Because the material softens after initiation, the maximum simulated stresses in Fig. 5 matched the input initiation stress and did not depend on whether or not the damage parameters are coupled. After initiation, however, deformation is strongly affected by damage mechanics method. Figure 6 compares A.  $\delta = d\varepsilon_{eff}$  for isotropic damage mechanics to  $\delta_s$  for B. uncoupled cuboid/elliptical surface, C. coupled cuboid/elliptical surface, and D. coupled ovoid surface, all for  $f = 0.2$  at 3.4% strain (which was strain just before ovoid surface failed by decohesion). The right side of Fig. 6 shows the deformed shape of one particle from the middle of the damaged region. By isotropic damage mechanics, failure occurs at a high stress ( $\sigma_{max} = 15.87$  MPa) followed by rapid tensile failure at about 2% strain. Subsequent post-failure deformation effectively causes cracking displacement in the direction of the loading. All anisotropic damage mechanics methods failed at about 6 MPa with a crack angle close to  $45^\circ$  (see  $f = 0.2$  in Fig. 5). Because uncoupled methods that initiate in shear will only soften in shear, the post-failure deformation corresponds to necking with crack-opening displacement limited to shear slippage (see Fig. 6B). This damaging process is closer to shear plasticity theory than to crack propagation. By coupling the damage parameters, the cuboid/elliptical failure surface shows partial coalescence of damage into a  $45^\circ$  crack with some normal crack opening; the shear damage is now coupled to normal damage thereby allowing the crack to open (see Fig. 6C). An ovoid surface with coupled damage parameters provides the most compelling simulation for tensile loading of a crack initiated in shear (see Fig. 6D). A clear crack forms at  $45^\circ$  and that crack opens under subsequent axial loading in the direction of the loading. Two results are clear — 1. coupling of damage parameters provides the best description of failure by crack initiation and opening; 2. an ovoid surface provides clearer crack definition than a cuboid or elliptical failure surface.

#### 4.3. Pressure Dependence

A 3D example for pressure-dependent damage mechanics is axial compression while the lateral surfaces are loaded to constant compressive stress  $p_T$ . The shear initiation stress was assumed

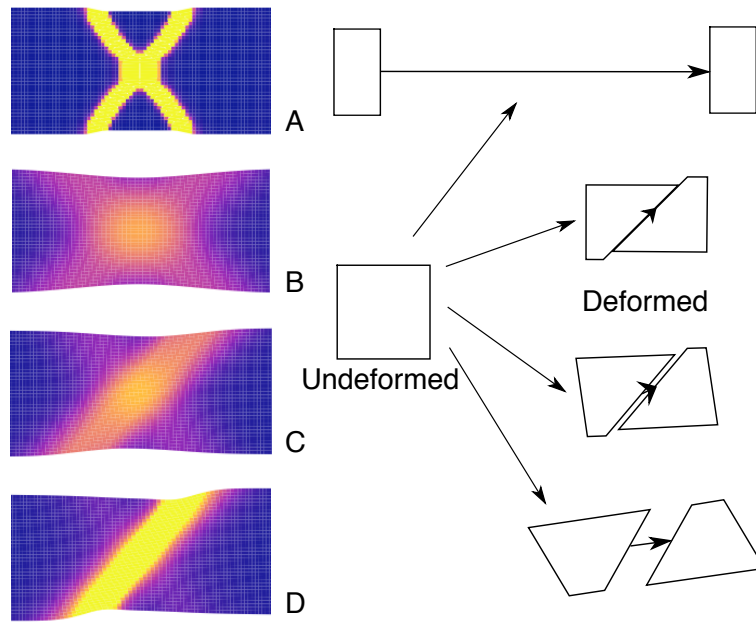


Figure 6. Damage states for failure that initiates in shear using A. isotropic damage mechanics, B. uncoupled cuboid/elliptical surface, C. coupled cuboid/elliptical surface, and D. coupled ovoid surface, all for  $f = 0.2$ . The left plots  $\delta_s$  at 3.4% strain for range of 0 (dark) to 0.5 (light) (note that isotropic damage mechanics plots  $\delta = d\varepsilon_{eff}$  instead). The right shows the deformed shape of a particle in the middle of the necked region with a crack at the simulated crack angle. The two halves of the deformed particles are shifted by the simulated crack opening displacement. All deformed particles are enlarged to the same relative scale and an undeformed particle is shown for reference.

to have pressure dependence

$$\tau_c(P) = \tau_c(0) \left( 1 + \frac{P}{\sigma_h} \right) \tag{32}$$

where  $\sigma_h$  is hydrostatic tension that causes shear strength to reach zero when  $P = -\sigma_h$ .  $G_{Ic}$ ,  $G_{IIc}$ , and  $\sigma_c$  were assumed to be pressure independent, which implies  $\delta_s^{(c)}$  decreases as  $P$  increases. Because ADaM requires positive initiation stress for all pressures,  $\sigma_c$  must be less than  $\sigma_h$  such that tensile initiation occurs before reaching zero shear strength. A  $12 \times 8 \times 8$  mm bar was pressurized on lateral surfaces by ramping from 0 to various  $p_T$  followed by loading in compression in the long direction. The initial pressurization and subsequent axial loading were done at 1 m/s (0.1% of the materials wave speed). The MPM grid used 0.8 mm cells with 8 particle per cell. All other properties were the same as in the previous section. In compression, failure initiates at compressive stress  $\sigma$  when  $|\sigma - p_T| = 2\tau_c(P)$  where  $P = (\sigma + 2p_T)/3$ . Using the shear strength in Eq. (32), failure initiation is expected when

$$\sigma = \frac{2\tau_c(0) + p_T \left( 1 + \frac{4\tau_c(0)}{3\sigma_h} \right)}{1 - \frac{2\tau_c(0)}{3\sigma_h}}$$

Figure 7A compares MPM simulations (symbols) for initiation of failure to this expectation (solid lines) for  $\sigma_h = 15$  MPa and  $\sigma_h = \infty$  (i.e., pressure independent); the results agree.

The stress-strain curves are shown in Fig. 7B. Because the axial ends were held fixed during initial pressurization, the axial compressive stress initially increased or decreased for  $p_T > 0$  or  $p_T < 0$ , respectively, before linearly increasing during subsequent axial loading. After damage initiation, the slopes decreased, but compression loading, with contact modeling, continues to increase. The post-failure slopes for pressure-dependent (solid curves) and pressure-independent (dashed curves) strength differed slightly. These simulations revealed the

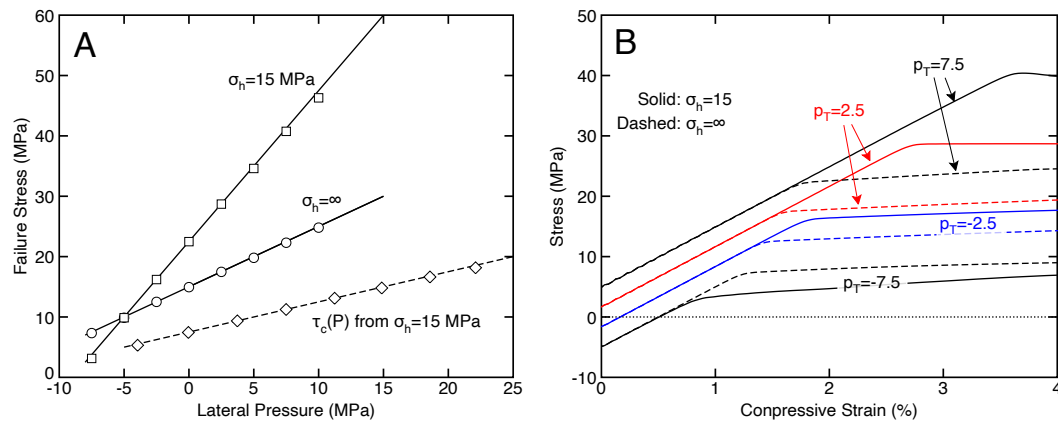


Figure 7. A. Compressive stress (unsigned) at initiation of failure for  $\sigma_h = 15$  MPa or  $\sigma_h = \infty$  (solid lines). The dashed line and symbols are expectation (dashed line) compared is back-calculation of  $\tau_c(P)$  by treating the  $\sigma_h = 15$  MPa values as experimental results (symbols). B. Compressive stress-strain curves during damage evolution for  $\sigma_h = 15$  MPa (solid lines) or  $\sigma_h = \infty$  (dashed lines) for lateral pressures  $p_T = 7.5$ ,  $2.5$ , or  $-7.5$  MPa.

importance of modeling initiation and evolution of damage by the same criterion. Any damage mechanics model that adds pressure dependence to the initiation failure criterion, but fails to consistently include that pressure dependence throughout damage evolution developed a discontinuity at the onset of damage. The smooth transitions in Fig. 7B are result of using the same failure surface for both initiation and evolution.

This loading example doubles as an experimental method for measuring pressure dependence of shear strength. Each experimental result as a function of  $p_T$  returns one shear strength value for one pressure or  $\tau_c(P = (\sigma + 2p_T)/3) = 0.5|\sigma - p_T|$ . The diamond symbols in Fig. 7 treat the  $\sigma_h = 15$  MPa results as virtual experiments and extracts  $\tau_c(P)$ . This exercise returns the input linear shear dependence (the dashed line). Doing this calculation for actual experimental results would return shear-strength material properties, including nonlinear responses.

The  $d\alpha = dP$  increment needed by sub-step #2 above is  $dP = -K(de - d\epsilon_{c,xx})$  where  $K$  is bulk modulus and  $de$  is trace of the incremental strain tensor. This relation causes a problem when using coupled methods because  $d\epsilon_{c,xx}$  is both an input to sub-step #2 and an output of sub-step #3. This problem was solved by an iterative algorithm. First, assume elastic deformation such that  $d\epsilon_{c,xx} = d d\epsilon_n$  and evaluate damage evolution resulting in a new result for  $d\epsilon_{c,xx}$ . Then, if output and input  $d\epsilon_{c,xx}$  are sufficiently close, the calculations are done. Otherwise recalculate  $dP$  using updated  $d\epsilon_{c,xx}$ , return to sub-step #2, and repeat until converged.

#### 4.4. Glass Sphere Impact

One last example simulated impact of soda lime glass spheres on an aluminum oxide anvil. Experimental results for 4.7 mm diameter spheres at various velocities show a variety of failure modes [22]. At low velocity ( $<25$  m/s) the impact site develops Hertzian cracks with a significant portion of the impact site “pulverized by the impact.” At intermediate velocities, failure changes to radial cracks (*i.e.*, the sphere fragments like an orange into slices) and a crushed cone at the impact site remained as an intact fragment. Finally, at very high velocities the spheres “disintegrated into a powder” [22]. This change from pulverized impact site to an intact, crushed cone suggests pressure-dependent damage such that less impact-site damage occurs when impacted at higher rates that induce higher pressures.

To see if pressure-dependent damage mechanics displays similar failure modes, 3D simulations were done at 30 m/s. Soda lime glass was estimated to have  $E = 72$  GPa,  $\nu = 0.208$ ,  $\rho = 2.52$  g/cm<sup>3</sup>,  $\sigma_c = 60$  MPa,  $K_{Ic} = 0.75$  MPa $\sqrt{m}$  (or  $G_{Ic} = 45$  J/m<sup>2</sup>), and  $K_{IIc} = \sqrt{10} \times K_{Ic}$

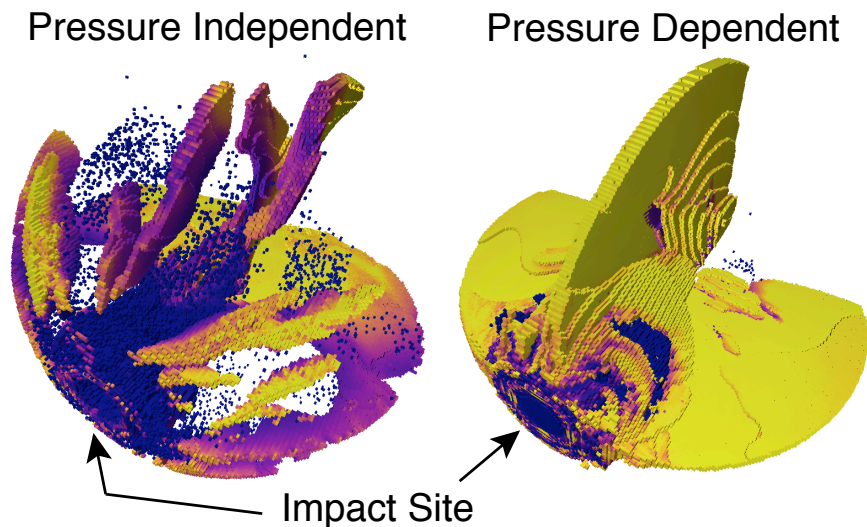


Figure 8. The geometry of the cracks (*i.e.*, failed particles only) for pressure-independent (left) or pressure-dependent (right) shear strength. The shading indicates failure mode from purple (or dark) for pure shear to yellow (or light) for pure tension. All remaining spherical spaces are filled with non-failed particles. The pressure-dependent cracks indicate failure of the sphere into four “orange slices.”

[23, 24]. To model pressure dependence,  $\tau_c$  was assumed to increase by a sigmoidal shape:

$$\tau_c(P) = \tau_0 + \frac{\tau_{max} - \tau_0}{1 + e^{-\ln 2(P - P_{mid})/P_{1/3}}}$$

where  $\tau_0 = 45$  MPa,  $\tau_{max} = 240$  MPa,  $P_{mid} = 25$  MPa and  $P_{1/3} = 10$  MPa. This strength transitions from  $\tau_0$  at low pressure to  $\tau_{max}$  at high pressure, passing through  $(\tau_0 + \tau_{max})/2$  at  $P_{mid}$ , and 1/3 of the strength change occurs within  $P_{mid} \pm P_{1/3}$ . The aluminum oxide anvil was assumed to be linear elastic with  $E = 300$  GPa,  $\nu = 0.22$ ,  $\rho = 3.89$  g/cm<sup>3</sup>. These simulations were qualitative because material properties were uncertain (*e.g.*, no mode II toughness for soda lime glass could be found). A sigmoidal shape that limits the maximum strength was arbitrary and used to avoid these brittle material simulations becoming unstable due to insufficient spatial resolution (*i.e.*  $\Delta x_p < \eta_s(K_{IIc}/\tau_c)^2$  decreases rapidly if  $\tau_c(P)$  increases too much). The simulations used full mass-matrix methods (FMPM(2)) with quadratic spline shape functions (B2CPDI) [21]. To avoid artifacts, the anvil had to be thick enough to avoid reflected waves during the simulation (for 7  $\mu$ s). This was achieved by using larger particles in the anvil remote from the impact site using a Tartan grid [25]. The sphere and impact site were discretized with a regular grid having 224 particles across the sphere’s diameter (20 million particles).

Figure 8 compares damage state 4  $\mu$ s into the impact event for pressure-independent and pressure-dependent material properties. The figure shows only failed particles colored (or shaded) to indicate their failure mode from purple (or dark) for pure shear failure to yellow (or light) for pure tensile failure. Empty spherical space is filled with still-intact particles. Indeed, adding pressure dependence to  $\tau_c(P)$  has a profound effect on failure mode. With no pressure dependence, shear failure dominates and is rather diffuse. By adding pressure dependence, the failure resembles experimental results that develop radial cracks breaking the sphere into orange-slice fragments. The impact site still sustains significant damage but has evidence of a “crushed cone” by virtue of reduced shear damage.

#### 4.5. Additional Options

This paper derives general ADaM by defining  $\mathbf{D}$  as a tensor that partitions total strain into elastic and cracking strains and includes new methods for coupling damage parameters and modeling

materials where failure depends on other variables. This section remarks on additional options or ideas for future work.

*Determining Initiation and the Crack Normal:* The cost of seeking a more realistic description of cracks using ADaM vs. isotropic damage mechanics is that ADaM must determine both when a crack initiates and its normal vector. All calculations in this paper used particle stresses — an approach that raises two issues. First in any discrete method (e.g., both MPM and FEM), local particle (or element) stresses depend on resolution. For example, a discrete model of stresses near a crack tip, where theoretical stress is infinite, will get larger stresses as particle sizes get smaller. Thus, any discrete modeling that relies on local stress must treat initiation stress as a resolution-dependent property [11]. Accepting resolution dependence is workable when using a regular grid (as commonly done in MPM), but problematic in methods that allow damage to propagate through regions with different resolutions. Second, inaccuracies or noise in local stress may cause inaccurate crack normals. When ADaM simulations encounter problems, those problems always appear to be associated with crack normals. Those problems did not occur in examples above or in prior work [10, 11, 12]. A promising solution if problems arise is to switch from particle stresses to non-local stresses or to base initiation and crack normal on stress averaged over a volume with some input non-local radius. This radius would remain constant as resolution changes. Preliminary results suggest this change can minimize resolution dependence and improve crack normal calculations (it will be developed in a future publication).

*Diffuse Damage:* In ADaM, softening is limited to directions normal and shear to the crack plane. While this feature is beneficial for representing cracks, it might not account for diffuse damage that causes softening in other directions. A potential addition would to add diffuse damage to the damage tensor or write

$$\mathbf{D}_{total} = \alpha \mathbf{D} + (1 - \alpha) \mathbf{D}_{diffuse}$$

where  $\mathbf{D}$  is from Eq. (12),  $\mathbf{D}_{diffuse}$  is due to diffuse damage, and  $\alpha$  is a mixing parameter. I suggest  $\mathbf{D}_{diffuse}$  should modify isotropic damage tensor of  $\mathbf{D}_{iso} = d\mathbf{I}$  to remain diagonal but use  $H(\sigma_{xx})d$  for normal terms and  $d$  for shear terms. Most of the analysis of this paper would remain the same. The damage evolution would continue to be based on crack tractions allowing modeling of mode I and mode II failures. The main difference would be that the update for stresses not in the traction vector would reflect diffuse damage. The chief drawback would be deciding how to choose the new mixing parameter  $\alpha$ , but it should be anticipated to be near 1.

*Coupled Plasticity:* By strain-partitioning, the current  $\mathbf{D}$  can find incremental bulk strain from total incremental strain using  $d\boldsymbol{\varepsilon}_{bulk} = (\mathbf{I} - \mathbf{D})d\boldsymbol{\varepsilon}$ . The above equations treated  $d\boldsymbol{\varepsilon}_{bulk}$  as an elastic strain, but one could, for example, model the bulk as an elastic-plastic material as follows: 1. Each time step would do plasticity modeling using  $d\boldsymbol{\varepsilon}_{bulk}$  resulting in a stress increment and a partitioning of  $d\boldsymbol{\varepsilon}_{bulk}$  into bulk elastic and plastic strain increments. 2. Once done, subtract plastic strain increment from total strain increment and evaluate damage evolution by elastic-material methods.

*Coupled Heat Conduction:* When elasticity is coupled to the heat equation, changes in volume induce an adiabatic change in temperature,  $dT_{dS=0}$ , which for an isotropic material is

$$\frac{dT_{dS=0}}{T} = -\frac{K\alpha}{\rho C_v} \frac{\Delta V}{V}$$

where  $K$  is bulk modulus,  $\alpha$  is volumetric thermal expansion coefficient,  $\rho$  is density,  $C_v$  is constant-volume heat capacity, and  $\Delta V/V$  is volumetric strain [26]. If this coupling is based on total strain, however, crack opening would be misinterpreted as an increase in volume inducing cooling. Instead,  $dT_{dS=0}$  must be calculated solely from the volumetric strain increment in  $d\boldsymbol{\varepsilon}_{bulk}$ . The cracks implied by ADaM likely also affect heat conduction. This effect could be modeled by changing the thermal conductivity tensor as a function of damage state. For an isotropic material, the tensor should evolve to an anisotropic tensor with reduced conductivity normal to the crack plane.

*Large Deformation Theory:* Extension to large deformation theory should start by defining  $\mathbf{D}$  as deformation-partitioning tensor. For example, 1D elongation could be partitioned into  $\lambda = \lambda_c \lambda_e$  or a product cracking and elastic elongations. Defining  $D$  as fraction of total length change due to crack opening results in  $(\lambda - \lambda_e) = D(\lambda - 1)$  (which reverts to  $\varepsilon_c = D\varepsilon$  for small strains). As  $D$  evolves from 0 to 1,  $\lambda_e$  evolves from  $\lambda$  to 1 while  $\lambda_c$  evolves from 1 to  $\lambda$ . 1D methods would evolve  $D$  by keeping Cauchy stress less than or equal to a strength model defined as a function of maximum  $\lambda_c$ . Extension to 3D might define a damage tensor by  $(\mathbf{F} - \mathbf{F}_e) = \mathbf{D}(\mathbf{F} - \mathbf{I})$  where  $\mathbf{F} = \mathbf{F}_c \mathbf{F}_e$  is total deformation tensor as a product of deformation tensors due to cracking or elastic deformations. The form of  $\mathbf{D}$  would be determined by large-deformation description of smeared cracks.

*Anisotropic Materials:* The above damage mechanics completely accounts for orthotropic materials, but implementation needs direction-dependent traction failure surfaces that cannot be based on principal stresses. A viable approach for orthotropic materials is:

- Resolve stress into components along material symmetry planes resulting in 9 strength models (3 for normal stress and 6 for shear stresses) with associated toughnesses.
- When damage initiates, assume the damage normal is always along a material symmetry plane. This restriction keeps the material orthotropic in the CAS. It is consistent with many (not all) failure modes in anisotropic materials. Note: the need for 6 shear strength models is that each shear plane needs two strengths to model cracks with normals in the two material directions in that plane. In practice, all shear cracks in that plane will initiate in the weaker direction.

Although failure surfaces in nine strength models are problematic, a cubic failure surface for each material symmetry direction works reasonably well. If a cubic surface is inadequate, this analysis could be amended to use other shapes, which may not be elliptical shapes. Because damage updates depend on  $S(\mathbf{c})$  through Eq. (14), switching to new failure surfaces would retain stress-strain curve in Eq. (2) and  $\mathbf{D}$  in Eq. (12), but would need to derive new update equations. If an orthotropic material fails with crack normal that is not in a material symmetry direction,  $\mathbf{C}$  in the CAS would have non-zero terms associated with a generally-anisotropic material. Modeling such behavior may require both additional constraints to determine  $\mathbf{D}$  and coupling of the strength models (e.g.,  $F_n(\delta_n, \delta_{xy}, \delta_{xz})$ ).

## 5. CONCLUSIONS

The “mechanics” of anisotropic damage mechanics (ADaM) is fully determined by interpreting  $\mathbf{D}$  as a fourth-rank tensor that partitions total strain,  $\boldsymbol{\varepsilon}$ , into bulk material strain,  $\boldsymbol{\varepsilon}_{bulk}$ , and cracking strain associated with crack opening,  $\boldsymbol{\varepsilon}_c$ , by  $\boldsymbol{\varepsilon}_c = \mathbf{D}\boldsymbol{\varepsilon}$ . ADaM implementation is centered around a postulated *traction failure surface* modeling crack traction conditions that induce evolution of damage with these properties:

*Three Strength Models:* The traction failure surface is defined by  $F_n$ ,  $F_{xy}$ , and  $F_{xz}$ , which are associated with three components of crack traction, evolve as damage variables associated with three crack-opening directions,  $\delta_n$ ,  $\delta_{xy}$ , and  $\delta_{xz}$ , evolve, and allow the model to partition tensile and shear failure. Damage initiation occurs when the traction on any virtual crack plane reaches this failure surface for undamaged strength properties (and orientation of that virtual plane defines the crack normal for subsequent damage evolution).

*Damage Evolution:* Damage evolves whenever trial traction causes  $\Phi(\mathbf{T}^{(trial)}, \mathbf{c}) > 0$  and the increment in damage is found by returning to an evolved surface such that  $\Phi(\mathbf{T} + d\mathbf{T}, \mathbf{c} + d\mathbf{c}) = 0$ . Returning to the evolved surface along a path toward the origin assures that all crack tractions simultaneously reach zero at failure and couples the damage parameters needed to define  $\mathbf{D}$  into a single damage parameter. The tensile-failure example shows that coupling damage parameters is the preferred approach to modeling materials that fail by crack formation and propagation.

*Damage Material Properties:* The input material properties are strengths and toughness needed to define the axes of the traction failure surface. For isotropic materials these reduce to just normal and shear strength models; anisotropic materials need strength models for each possible failure direction. The special theory of damage mechanics assumes these strength models depend only on the damage state. The general theory is needed to model materials where strength depends on other variables. The pressure-dependent examples suggest the general theory has potential for modeling real-world effects that could not be modeled by prior damage mechanics methods.

## APPENDIX I

Instead of deriving damage evolution from a strength model that depends on  $\delta$ , damage mechanics could proceed using strength models that depend on  $D$  and postulate  $D$  evolution laws [13, 27]. These two approaches are identical provided the strength models and evolution laws are consistent.

The first question is — given  $F(\delta)$ , what is the corresponding  $F(D)$  strength model? The general result is

$$F(D) = F(\delta^{-1}(D))$$

where  $\delta^{-1}(D)$  is inverse to last relation in Eq. (4). For example, a linear strength model with  $F(\delta) = E\varepsilon_0(1 - \delta/\delta^{(c)})$  (where  $\varepsilon_0$  is strain to initiate damage), leads to non-linear  $F(D)$  strength model:

$$F(D) = E\varepsilon_0 \frac{(1-D)\delta^{(c)}}{\delta^{(c)} + D(\varepsilon_0 - \delta^{(c)})}$$

Most non-linear  $F(\delta)$  models will need numerical methods to determine  $F(D)$ . An approach that starts with  $F(D)$  would revise Eq. (4) to

$$\sigma = E(1-D)\varepsilon_i = F(D) \implies \varepsilon_i = \frac{F(D)}{E(1-D)} \implies \delta = D\varepsilon_i = \frac{D}{1-D} \frac{F(D)}{E}$$

Now given  $F(D)$ , the corresponding strength model inverts this last relation to give  $F(\delta) = F(D^{-1}(\delta))$ . For example, choosing a linear  $F(D) = E\varepsilon_0(1-D)$  results in  $F(\delta) = E\varepsilon_0(1 - \delta/\varepsilon_0)$  that corresponds to brittle elastic response (*i.e.*,  $\delta^{(c)} = \varepsilon_0$ ); this model is unstable and therefore not useful to damage mechanics. In general, choosing  $F(D)$  is difficult because  $D$  lacks the physical interpretation available by relating  $\delta$  in 1D to the maximum cracking strain. Damage mechanics is better implemented by choosing  $F(\delta)$  models.

The second questions is — given an  $F(\delta)$  strength model, what is the corresponding  $D$  evolution law? During one-dimensional damage evolution, total strain and  $D$  in terms of that strain are:

$$\varepsilon = \delta + \frac{F(\delta)}{E} \implies D = \frac{\delta^{-1}(\varepsilon)}{\varepsilon}$$

where  $\delta^{-1}(\varepsilon)$  is inverse of the first equation. The  $D$  evolution law during monotonically increasing strain in terms of a strength model embedded in  $\delta^{-1}(\varepsilon)$  becomes

$$\frac{dD}{d\varepsilon} = \frac{\varepsilon \frac{d\delta^{-1}(\varepsilon)}{d\varepsilon} - \delta^{-1}(\varepsilon)}{\varepsilon^2}$$

For example, a linear strength model leads to evolution laws for  $D$  and  $\delta$  when  $\varepsilon > \varepsilon_0$  as:

$$\delta^{-1}(\varepsilon) = \frac{\delta^{(c)}(\varepsilon - \varepsilon_0)}{\delta^{(c)} - \varepsilon_0}, \quad D = \frac{\delta^{(c)}}{\delta^{(c)} - \varepsilon_0} \left(1 - \frac{\varepsilon_0}{\varepsilon}\right), \quad \frac{dD}{d\varepsilon} = \frac{\delta^{(c)}\varepsilon_0}{(\delta^{(c)} - \varepsilon_0)\varepsilon^2}, \quad \frac{d\delta}{d\varepsilon} = \frac{\delta^{(c)}}{\delta^{(c)} - \varepsilon_0},$$

The  $D$  evolution law is nonlinear:  $D$  evolves rapidly after initiation but more slowly near failure. In contrast,  $\delta$  evolves at a constant rate. Although either approach works in 1D, evolution using strength models and  $\delta$  is preferred in 3D and in the general theory.

## APPENDIX II

This appendix considers various methods for returning a trial traction that exceeds failure surface to the evolved surface in Fig. 3. A common method in plasticity theory is to return normal to the evolved surface. By this approach, the second equation for damage evolution is

$$\|\mathbf{r} \times \mathbf{n}\| = 0 \quad \text{where} \quad \hat{\mathbf{n}} \|\hat{\mathbf{n}}\| = \left( \frac{\tau_{xy}^{(trial)} - r_y}{F_{xy}^2 (\delta_{xy} + d\delta_{xy})}, \frac{\tau_{xz}^{(trial)} - r_z}{F_{xz}^2 (\delta_{xz} + d\delta_{xz})} \right)$$

is normal vector to the evolved ellipse. Expanding in a Taylor's series and keeping first-order terms, this coupling equation simplifies to

$$C_{66}(1 - d_{xy})\varphi_{xy}(\delta_{xy})d\delta_{xy} = C_{55}(1 - d_{xz})\varphi_{xz}(\delta_{xz})d\delta_{xz}$$

For an isotropic material, this coupling again leads to  $d_{xy} = d_{xz}$ , but for anisotropic materials, the damage parameters may differ. Because the coupling equation leads to some damage in both directions even during uniaxial shear loading, a model with  $d_{xy} \neq d_{xz}$  could fail by  $x$ - $z$  shear strength even when loaded with  $\tau_{xz} = 0$ . This non-physical response again suggests  $d_{xy}$  and  $d_{xz}$  should be linked. Note that Ref. [10] proposes shear coupling by this normal return method. Although that approach is valid for the isotropic materials, that paper has errors in calculating the return path. Its coupling equation is different and does not result in  $d_{xy} = d_{xz}$ . In brief, the uncoupled options in Ref. [10] are correct, but its coupling equations must be replaced by Eq. (20).

By a fracture mechanics view of ADaM, damage evolution is energy balance. Perhaps the return vector should maximize dissipated energy? When this option was tried, however, the energy extremum was found to fall on the boundary for admissible increments in  $d\delta_{xy}$  and  $d\delta_{xz}$  and those boundaries sometimes result in physically-unacceptable solutions.

Finally, the return vector could be parallel to the trial shear traction. The second equation and its simplification after Taylor series expansion become

$$0 = \|\mathbf{r} \times \mathbf{T}_s^{(trial)}\| \quad \implies \quad \frac{\mathbb{R}_{xz}d\delta_{xz}}{1 - d_{xz}} = \frac{\mathbb{R}_{xy}d\delta_{xy}}{1 - d_{xy}}$$

At damage initiation,  $d_{xy} = d_{xz} = 0$  and the first update becomes  $d(d_{xz}) = \mathbb{R}_{xz}d\delta_{xz} = \mathbb{R}_{xy}d\delta_{xy} = d(d_{xy})$ . On the next step, the  $d$ 's will be equal and they will remain equal on all subsequent steps (*i.e.* this option links  $d_{xy} = d_{xz}$ ). In summary, coupling  $d_{xy}$  and  $d_{xz}$  physically corresponds to returning to the evolved surface in the direction of the origin and guarantees both shear traction components decay to zero at shear failure.

## ACKNOWLEDGEMENTS

This work was made possible by the endowment for the Richardson Chair in Wood Science and Forest Products.

## REFERENCES

1. Kachanov L. Time of rupture process under creep conditions. *Izv. Akad. Nauk SSR, Otd. Tekh. Nauk* 1958; **8**:26–31.
2. Chaboche J. Le concept de contrainte effective appliqué à l'élasticité et à la viscoplasticité en présence d'un endommagement anisotrope. *Mechanical Behavior of Anisotropic Solids / Comportment Mécanique des Solides Anisotropes*, Boehler JP (ed.). Springer Netherlands, 1979; 737–760.
3. Chaboche J. Anisotropic creep damage in the framework of continuum damage mechanics. *Nuclear Engineering and Design* 1984; **79**(3):309 – 319.
4. Ju JW. Isotropic and anisotropic damage variables in continuum damage mechanics. *Journal of Engineering Mechanics* 1990; **116**(12):2764–2770.
5. Chaboche JL. Development of continuum damage mechanics for elastic solids sustaining anisotropic and unilateral damage. *International Journal of Damage Mechanics* 1993; **2**(4):311–329.

6. Cervera M. A smeared-embedded mesh-corrected damage model for tensile cracking. *International Journal for Numerical Methods in Engineering* 2008; **76**(12):1930–1954, doi:<https://doi.org/10.1002/nme.2388>.
7. Jirásek M, Zimmermann T. Analysis of rotating crack model. *Journal of Engineering Mechanics* 1998; **124**(8):842–851, doi:10.1061/(ASCE)0733-9399(1998)124:8(842).
8. Cervera M. An orthotropic mesh corrected crack model. *Comput. Methods Appl. Mech. Engrg.* 2008; **197**:1603–1619.
9. Barbat G, Cervera M, Chiumenti M. Appraisal of planar, bending and twisting cracks in 3d with isotropic and orthotropic damage models. *International Journal of Fracture* 03 2018; **210**:1–35, doi:10.1007/s10704-018-0261-3.
10. Nairn JA, Hammerquist CC, Aimene YE. Numerical implementation of anisotropic damage mechanics. *Int. J. for Numerical Methods in Engineering* 2017; **112**(12):1846–1868.
11. Nairn JA. Direct comparison of anisotropic damage mechanics to fracture mechanics of explicit cracks. *Eng. Fract. Mech.* 2018; **203**:197–207.
12. Aimene Y, Hammerquist CC, Nairn JA, Ouenes A. 3d anisotropic damage mechanics for modeling interaction between hydraulic and natural fracture planes in a layered rock– application to eagle ford and wolfcamp. *Unconventional Resources Technology Conference (URTEC), Houston, Texas, USA, 23-25 July, 2018*.
13. Oliver J. Modelling strong discontinuities in solid mechanics via strain softening constitutive equations. Part 2: Numerical simulation. *International Journal for Numerical Methods in Engineering* 1996; **39**(21):3601–3623.
14. Oliver J. Modelling strong discontinuities in solid mechanics via strain softening constitutive equations. Part 1: Fundamentals. *International Journal for Numerical Methods in Engineering* 1996; **39**(21):3575–3600.
15. Nairn JA. Material point method (NairnMPM) and finite element analysis (NairnFEA) open-source software. [http://osupdocs.forestry.oregonstate.edu/index.php/Main\\_Page](http://osupdocs.forestry.oregonstate.edu/index.php/Main_Page) 2021.
16. de Souza Neto EA, Perić D, Owen DRJ. *Computational Methods for Plasticity: Theory and Applications*. John Wiley & Sons, 2008.
17. Li S, Thouless M, Waas A, Schroeder J, Zavattieri P. Mixed-mode cohesive-zone models for fracture of an adhesively bonded polymer–matrix composite. *Engineering Fracture Mechanics* 2006; **73**(1):64 – 78.
18. Nairn JA, Aimene YE. A re-evaluation of mixed-mode cohesive zone modeling based on strength concepts instead of traction laws. *Engineering Fracture Mechanics* 2021; **248**:107 704.
19. Stack Exchange. A circle inside and ellipse. <https://math.stackexchange.com/questions/1972994/a-circle-inside-an-ellipse> October 2016.
20. Sadeghirad A, Brannon RM, Burghardt J. A convected particle domain interpolation technique to extend applicability of the material point method for problems involving massive deformations. *Int. J. Num. Meth. Engrg.* 2011; **86**(12):1435–1456.
21. Nairn JA, Hammerquist CC. Material point method simulations using an approximate full mass matrix inverse. *Computer Methods in Applied Mechanics and Engineering* 2021; **337**:113 667.
22. Salman A, Gorham D. The fracture of glass spheres. *Powder Technology* 2000; **107**:179–185.
23. Wikipedia. Soda lime glass. <https://en.wikipedia.org/wiki/Soda>
24. Gong J, Chen Y, Li C. Statistical analysis of fracture toughness of soda-lime glass determined by indentation. *J. Non-Crystalline Solids* 2001; **279**:219–223.
25. Hammerquist CC, Nairn JA. Modeling nanoindentation using the material point method. *Journal of Materials Research* 05 2018; **33**:1369–1381.
26. Carlson DE. Linear thermoelasticity. *Mechanics of Solids*, vol. II, Truesdell C (ed.). Springer-Verlag, New York, 1984; 297–345.
27. Ladèveze P, Lubineau G. On a damage mesomodel for laminates: Micro-meso relationships, possibilities, and limits. *Comp Sci & Tech.* 2001; **61**:2149–2158.